Mónica Cristina Monteiro Martins

Towards an Integrated Electrocardiography System for Digital Stethoscopes

Thesis submitted to the University of Coimbra
for the degree of Master in Biomedical Engineering

July 2018

Universidade de Coimbra

• U C •

FCTUC FACULDADE DE CIÊNCIAS
E TECNOLOGIA
UNIVERSIDADE DE COIMBRA

Mónica Cristina Monteiro Martins

Towards an Integrated Electrocardiography System for Digital Stethoscopes

Thesis submitted to the
University of Coimbra for the degree of
Master in Biomedical Engineering

Supervisors:
Prof. Dr. Paulo Alexandre Vieira Crespo (Faculdade de Ciências e Tecnologia da Universidade de Coimbra)
Prof. Dr. Hugo Humberto Plácido da Silva (Instituto de Telecomunicações - Pólo de Lisboa)

Coimbra, 2018

This work was developed in collaboration with:

Instituto de Telecomunicações - Pólo de Lisboa

Faculdade de Ciências da Universidade do Porto

Universidade da Beira Interior

Acknowledgements

This work would have not been possible without the help and support of professors, colleagues, friends and family.

Firstly, I would like to express my gratitude and appreciation to my mentor, Hugo Silva, who tirelessly guided me through this project. For more than a year, Hugo made space for my questions, doubts and challenges, always returning on a positive note and with a visionary attitude. From electronics to data analysis, from programming to working with BITalino, and overall work-life experience, Hugo emerged me in all of it and prepared me for an exciting and promising future. Without a doubt, he has been present throughout my work and has supported, both me and my own vision and goals. Also, to my professor and mentor, Paulo Crespo, thank you for your relaxed attitude towards the elaboration of this thesis, and for helping with all things logistic when I was away. Both have showed a positive attitude towards my work and have congratulated me for all the small achievements attained leading up to this final work.

Secondly, for all the continuous support and time, I would like to thank Margarida Reis, who made me feel part of the IT team and taught me to step outside of my comfort zone. To Diana Baptista, for all the tips and advises on Python and electrocardiogram signal processing, thank you. Also, I would like to thank Joana Santos for the lessons on heart physiology and electrocardiogram experience. This project wouldn't be so complete without the help of these three ladies, who undoubtedly gave me the necessary knowledge to cross so many scientific areas and get to the results I've had.

Furthermore, I want to thank Professor Ana Fred and the Pattern and Image Analysis group (PIA) for welcoming me into this project and for providing me with the needed resources. To Cristina Oliveira and Pedro Gomes, from Instituto de Telecomunicações do Porto, thank you for assisting in the diaphragms test, in order to choose the most appropriate one for this project's prototypes, as well as for guiding

me in the auscultation process for signal acquisition. I would also like to thank Professor Ricardo Baptista and Miguel Rocha, from Escola Superior de Tecnologia do Instituto Politécnico de Setúbal, for assisting in the conception of the final 3D model for the developed system.

To all my generous and uplifting volunteers, I'm so grateful for your help and time. To the ones who have repeatedly let me record signals, thank you for your patience and entertaining conversations.

This work was partially developed under the Portuguese Foundation for Science and Technology, grant PTDC/EEI-SII/7092/2014 LearnBig and under the IT - Instituto de Telecomunicações grant UID/50008 SmartHeart, and therefore, I want to, once more, thank my mentor Hugo for allowing this and giving me the opportunity of not only being part of a revolutionary project, but also to be granted a scholarship and be financially supported while finishing my degree.

Last but not least, I want to express my gratitude to my dear loved ones, who made this experience outstandingly worthwhile and memorable. To Vasco, who always encouraged me to fight for my craziest dreams, never question my abilities and to always believe in myself, my deep thanks, for both your presence and love. To Carolina and João (Oliveira), for always having my back and keeping me company throughout these insane months, thank you. The bond will never be broken and the love will never be forgotten. To my dear friend Mélanie, thank you for your unconditional love and support, for always checking in and helping me get through the toughest times.

Finally, I would like to thank my parents, who gave me the opportunity to improve my education, who gave me the support and encouragement to pursue my (rather odd) ambitions, and always keep learning throughout my experiences. I am deeply grateful for your presence in my life and I will never take that for granted. I'm sorry for the absence over these past few months and thank you for teaching and guiding me through life. Honestly, thank you for everything.

Resumo

As doenças cardiovasculares são a principal causa de morte a nível mundial. Seja por falta de cuidado e preocupação com o estilo de vida, ou por uma doença pré-existente, o impacto das doenças cardíacas na sociedade atual é deveras alarmante. A prevenção, por sua vez, desempenha um papel crucial no que diz respeito à recuperação do estado de saúde da população. Esta pode passar por adotar uma forma mais consciente de viver ou pela monitorização regular do sistema cardiovascular. No entanto, os exames médicos rotineiros que permitem diagnosticar e controlar estas condições, requerem uma suspeita prévia e uma prescrição direcionada por parte da entidade médica responsável pelo paciente. Neste sentido, a abordagem atual tem as suas limitações e pode impedir a deteção precoce de anomalias cardíacas. Este trabalho apresenta uma abordagem alternativa para diagnóstico de doenças cardiovasculares, por meio de monitorização de auscultação e eletrocardiograma, incorporado num sistema único. Trata-se de um dispositivo inovador que permite a aquisição de sinais de eletrocardiograma ao longo dos cinco pontos de auscultação médica. Tem o intuito de ser incorporado num estetoscópio digital de uso corrente e, assim, permitir adquirir e analisar sinais de fonocardiograma e eletrocardiograma numa utilização única, seguindo as normas de uso de um estetoscópio regular. O foco deste trabalho foi a conceção e validação de dois protótipos na aquisição de sinais de eletrocardiograma nos pontos de auscultação médica, para posterior incorporação num estetoscópio digital, por meio do estudo de métricas adequadas que permitam avaliar a semelhança entre as ondas de um dispositivo de referência e as dos novos sistemas. Os resultados estão espelhados no protótipo SmartHeart; um acessório inovador, prático e ergonómico, de baixo custo e escalável à prática médica quotidiana.

Palavras-chave: Doenças cardiovasculares, Eletrocardiograma, Fonocardiograma, Estetoscópio digital, Integração de sistemas

Abstract

Cardiovascular diseases are the number one cause of death worldwide. Whether due to a careless lifestyle or to a pre-existing health condition, the impact of heart diseases in our society is undoubtedly alarming. Prevention, on the other hand, plays a crucial part in reclaiming the population's health back. Prevention goes from adopting a more conscious way of living, to regular monitorization of the cardiovascular system. However, routine exams that allow the diagnosis and control of such conditions, require a medical suspicion beforehand, and a medical prescription on behalf of the encharged healthcare professional. Therefore, this approach has several limitations and can prevent early detection of cardiac pathologies. This work presents a new approach to diagnose cardiovascular diseases, through auscultation and electrocardiogram monitoring, integrated in a single device. It is an innovative device that collects electrocardiogram signals throughout the five main medical auscultation points. It intends to be incorporated in a commonly used digital stethoscope and, therefore, allow analysis and acquisition of both phonocardiogram and electrocardiogram signals in a single pass, following the policy rules of a regular stethoscope usage. The purpose of this project was the development and validation of two prototypes in the acquisition of electrocardiogram signals on the medical auscultation points, in order to hereafter integrate it into a digital stethoscope, through adequate metrics that allow the evaluation of similarities between waveforms from a gold standard device and the ones obtained with the new systems. The final results can be seen in the SmartHeart prototype; an innovative, practical, and ergonomic accessory, which is also low cost and scalable to the everyday medical practice.

Key words: Cardiovascular diseases, Electrocardiogram, Phonocardiogram, Digital stethoscope, Systems integration

Acronyms

AC Alternating current.
ADC Analog-to-digital converter.
Ag Silver.
AgCl Silver Chloride.
AuAgPl Gold-silver-platinum.
AV Atrioventricular.
aVF Augmented vector Foot.
aVL Augmented vector Left.
aVR Augmented vector Right.

CMRR Common-mode rejection ratio.
CT Computed tomography.
CVD Cardiovascular diseases.

ECG Electrocardiogram.

FDA Food and Drug Administration.
FIR Finite impulse response.

GE General Electrics.

HIPAA Health Insurance Portability and Accountability Act.

IMU Inertial measurement unit.

LAN Local area network.
LiPo Lithium-polymer.

MRI Magnetic resonance imaging.

PCG Phonocardiogram.
PLA Poly(lactic acid).

RMSE Root mean square error.

SA Sinoatrial.
SD Secure digital.

TPU Thermoplastic polyurethane.

VCC Voltage at the common collector (the operating voltage).

WHO World Health Organization.

XML Extensible markup language.

List of Figures

List of Tables

Contents

1

Introduction

1.1 Cardiology and Medical Terms

1.1.1 Cardiovascular Diseases (CVD)

According to the World Health Organization (WHO), cardiovascular diseases (CVD) are the leading cause of death in the world [7]. However, one interesting and unfortunate fact is that the majority of deaths due to CVD occur in low and middle-income countries. In these countries citizens usually have limited primary healthcare programmes [7], and therefore they do not have the same opportunities of early detection as high-income countries do. Consequently, healthcare costs per household are higher than if there was more prevention investment and the countries themselves have a heavy burden on their economy.

It is widely known that CVD have several risk factors and behaviours, such as smoking tobacco, having an unhealthy diet, excessive weight, being physically inactive or irresponsibly drinking alcohol. These, in turn, often lead to raised blood pressure, raised glucose, raised blood lipids, or obesity. Prevention by making people more aware of these is key, given that those who are already at risk, would benefit from early detection of CVD. This approach is also financially advantageous, in the sense that prevention is more cost-effective than treatment itself [7].

Besides general prevention measures that should be accounted for, regular heart monitoring is crucial in risk patients. Therefore, auscultation plays a major role in CVD's monitoring. Being a routine exam, performed in any typical appointment with a health professional, auscultation allows a quick preliminary evaluation of the patient's heart condition.

1.1.2 Phonocardiogram (PCG)

First reported in 1970, by Keefer, J. M.[8], phonocardiography allows the representation of the heart sounds obtained when performing auscultation. Its outcome is a phonocardiogram (PCG) and it results from the mechanical response to the electrical activity of the heart [1].

It is used as a complementary exam of auscultation, given that the latter relies on the human ear, which may not be sufficient for an accurate evaluation of the patient [9]. The main problem with this technique is that it is difficult to master [1]. Therefore, specialized healthcare professionals are required, in order to perform a standard medical evaluation, hence the importance of using digital stethoscopes, which tipically combine auscultation and phonocardiography [10]. Also, the fact that it does not allow the automated recording of any information, stands out as a major fault in the auscultation process.

The PCG exam provides information about the heart activity through its sounds, which are in the range [10, 750] Hz, therefore being low frequency. These sounds can be heard over 5 auscultation points, which are depicted in Figure 1.1: second intercostal space on the right parasternal line, second intercostal space in the left parasternal line, third intercostal space in the left parasternal line, lower left border of the sternum and fourth/fifth intercostal space in the left hemiclavicular line.

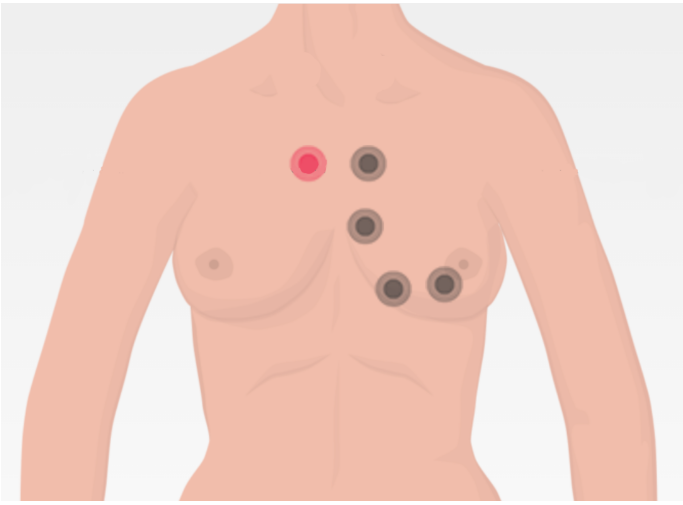

Figure 1.1: Main auscultation points. Image adapted from IS4Collection, IS4H - Interactive Systems for Healthcare©.

With PCG it is possible to determine the temporal localization of heart sounds, the number of their internal components, their frequency content and the significance of diastolic and systolic murmurs [9], with these being an extra or unusual sound

heard during a heartbeat and broadly classified as systolic, diastolic or continuous [10].

As set forth by [9] (see pg. 118 for additional information), "One of the first and most important phases in the analysis of heart sounds, is the segmentation of heart sounds. Heart sound segmentation partitions the PCG signals into cardiac cycles and further into S1 (first heart sound), systole, S2 (second heart sound) and diastole".

In a complete heart cycle, four phases can be identified, from which two sounds can be heard. Firstly there is the closure of the mitral and tricuspid valves (first sound - S1), then the systolic period, following the closure of the aortic and pulmonary valves (second sound - S2) and finally the diastolic period [9]. Also, S1's frequency is usally lower than S2's, and its duration longer [10]. See Figure 1.2 for an example of a typical PCG signal, annotated with the partitions of interest.

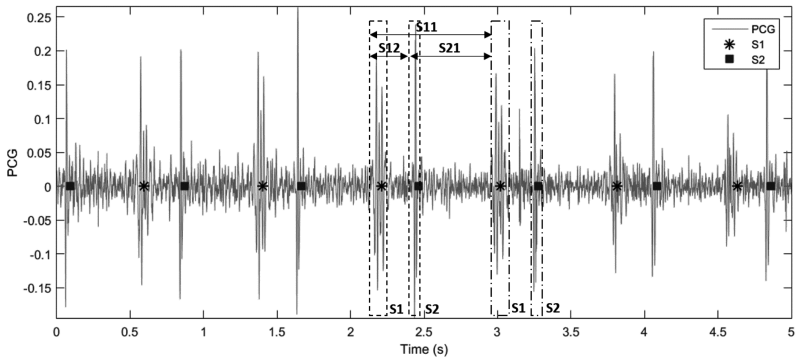

Figure 1.2: Example of a PCG exam and its segmentation. S11 corresponds to the heart cycle period, S12 to the systolic one, and S21 to the diastolic period (image from [1]).

If there is any abnormalty with the heart sounds, other sounds or murmurs can be heard between S1 and S2, indicating heart problems or diseases. Some pathologies that can be detected through PCG are hyperphonesis, murmurs, hypertension, mitral regurgitation, ventricular septal defect, hypertrophic cardiomyopathy, among several others [10].

The PCG exam has several advantages, such as being low cost, noninvasive and accurate for diagnosing some heart diseases [9]. It is also the fastest way to monitor patients, and of high importance outside of central hospitals, where not all medical exams can be taken [1]. There are many other options for medical heart evaluation, such as the electrocardiogram (ECG), echocardiogram, cardiac magnetic resonance imaging (MRI) and computed tomography (CT). However, these are expensive, need specialized personnel and are therefore not available everywhere [10].

In order to allow a more complete medical evaluation and circumvent the lack of diagnosis equipment, the PCG can be a compelling approach, especially considering that it is an extension to the standard auscultation procedures used in general medical practice. But then again, this exam also has its drawbacks. The heart sound has both high and low frequency signals, as well as low amplitude, making it necessary for the stethoscope to have a highly selective sensitivity. Also, the kind of data acquisition made with a stethoscope is highly affected by external noise (e.g. sounds produced in the surrounding environment to the subject), which can mostly interfere with the final diagnosis. Finally, the interpretation itself is higly subjective, depending on the healthcare professional and his/her experience, as well as hearing ability [10].

In conclusion, not only the need to use digital stethoscopes and automated signal processing techniques is evident, but also advances in this field are required in order to improve heart disease diagnosis, where new and top of the range machinery is not yet available [11]. Nevertheless, these needs have already motivated the development of such devices, as well as the ability of automated signal analysis of cardiac sounds [12], [13].

1.1.3 Electrocardiogram (ECG)

An electrocardiogram is a medical examination that allows the evaluation of the heart performance, through the study of its electrical activity. It is widely used due to the high benefit/cost ratio, and also for being an easily deployable noninvasive test. It allows the evaluation of multiple heart diseases, like poor blood flow (ischemia), heart attack or enlarged heart, just to name a few examples [14].

The heart is one of our most important organs and its walls are composed of cardiac muscle, the myocardium, which allows the heart to contract. The output of the ECG test consists of voltage variations as a function of time, in result of successive myocardium depolarization and repolarization events. This process creates electric fields, which reach the skin surface and, in turn, the electrodes placed on it. This process of depolarization and repolarization of cardiac cells occurs in a very similar way to that of other cells in the body. However, the duration of the cardiac muscle impulse is two orders of magnitude longer than that in either nerve cell or skeletal muscle [3]. Contraction of the heart occurs shortly after the action potential passes through the cardiac cells, as shown in Figure 1.3.

While at rest, like all remaning cells in our body, the cells of the cardiac muscle present a higher concentration of negative charges on the inside, and a majority of positive charges on their outside. The cardiac muscle contraction is the result of heart cells depolarization (inversion of the potential created by the charge concentration difference earlier mentioned). This process initiates in the sinoatrial node (SA node), that acts as a natural pacemaker, and continues throughout the other nodes. After the SA node, the atrioventricular node (AV node) appears, connecting the atria and the ventricles. Right after, the AV node gives rise to the Bundle of His and, more distally, this one separates into two branches, ending in the Purkinje fibers. Finally, the Purkinje fibers diverge and the impulse passes from the inner side of the ventricle walls to the outer side, due to cell-to-cell activation [3]. This conduction system of the heart can be seen in Figure 1.4 and, in terms of net depolarization vector, this sequence of events can be represented as depicted in Figure 1.5. The voltage recorded along a particular lead axis, at a particular time, is obtained by projecting the vector representing the magnitude and direction of depolarization. Also, the mean electrical axis is the average of all the instantaneous mean electrical vectors occurring sequentially during depolarization of the ventricles [4].

Therefore, depolarization is the trigger to the entire mechanism, which leads to an electrical potential variation. However, after the impulse passes through (beginning

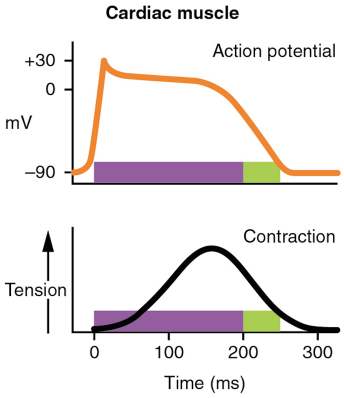

Figure 1.3: Difference between electrical activation and contraction times (image adapted from [2]).

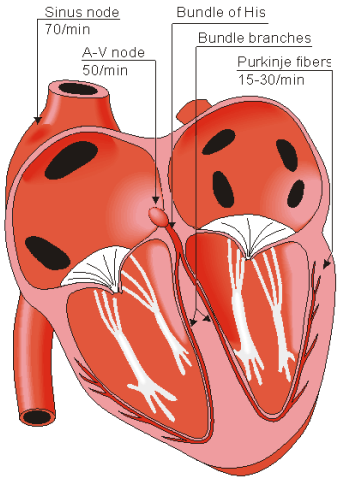

Figure 1.4: Conduction system of the heart (image from [3]).

in the nervous system), the cellular membranes of individual cells will return to rest, resulting in their repolarization (recovery).

As the heart is formed by thousands of cells, the depolarization process in each one will occur at different times. Therefore, an ECG is a relative and cumulative magnitude of all cells in depolarization. On the other hand, the amplitude of the obtained ECG signal is influenced by a number of factors: the myocardial mass (heart muscle mass), the net depolarization vector, the thickness, conductivity and resistivity of tissues around the heart (thorax region), and also by the distance between the electrodes and the myocardium. An example of how the mass influences the ECG acquisition is a patient with ventricular hypertrophy (relatively large myocardial mass). As consequence, this person's signal will probabily have a higher amplitude than that of a healhty subject [15]. Regardless, an ECG can be obtained with dif-

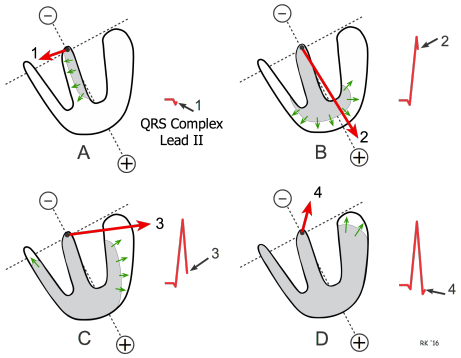

Figure 1.5: Mean electrical axis of depolarization within the ventricles. Example of electrode placement, representing Lead II (image from [4]).

ferent configurations and electrode locations, being that these will provide different perspectives of the electrical activity of the heart. For this reason, the signal that a combination of electrodes captures, with respect to the heart, may vary, but it is always an insight to the operation of the heart. The prototypical ECG heartbeat waveform is shown in Figure 1.6 (considering a healthy medical case).

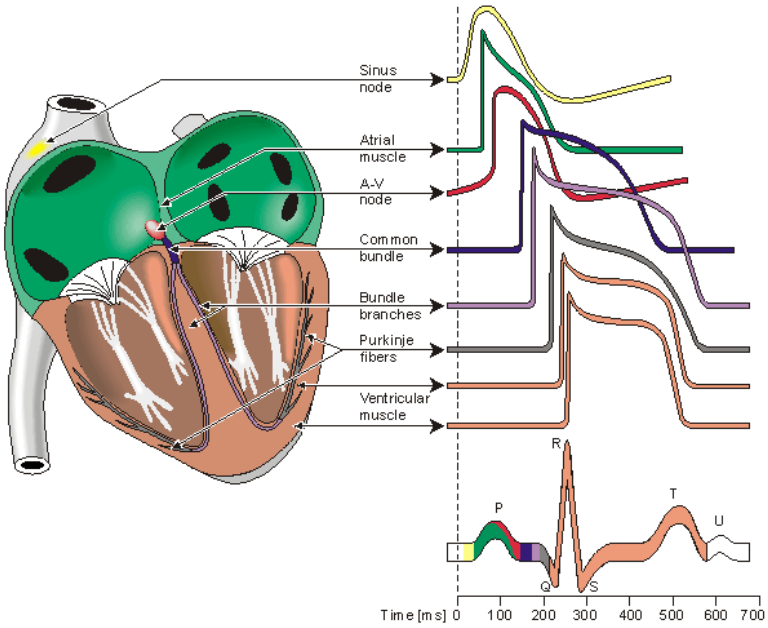

Figure 1.6: Different waveforms for different heart cells and their contribution to the prototypical heartbeat waveform (image from [3]).

This curve is highly relevant because timing, amplitude, and morphological ECG parameters can be derived from it, supporting diagnosis. From the ECG, the P wave can be seen, which represents the atrial depolarization, important to study the cardiac rhythm; the P-R interval follows, that measures the impulse conduction time through the atria, atrioventricular node and other fibers of the conduction system;

the QRS interval is next, which represents the beginning of ventricular contraction; followed by the Q-T interval, which is the time interval from when the ventricles begin their depolarization to the time when they have repolarized to their resting potentials; and finally, there is the S-T segment, which corresponds to a resting period, between depolarization and the beginning of repolarization.

It is also important to mention some basic interpretations that can be made from simple ECG characteristics. An electrical current going into the positive electrode will correspond to a positive deflexion on the ECG signal, while a depolarization current going the opposite way will result in a negative deflexion. On the other hand, a repolarization current that goes away from the electrode will result in a positive deflexion. A fast depolarization (or repolarization) is represented by a narrow curve, that becomes wider when the depolarization is slower. With this comes the need of a standard ECG, in a way that it can be equally interpreted by any professional, leaving no doubt or space for errors in the diagnosis.

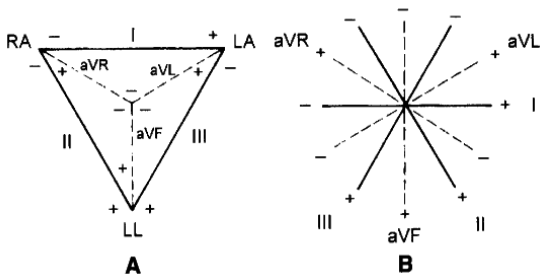

Figure 1.7: Augmented leads and leads I, II and III in Figure (A). Hexaxial reference limb system in Figure (B) (image from [5]).

With that purpose, Einthoven leads are used when dealing with ECG measurements. Figure 1.7 presents the system proposed by Einthoven, who idealized the cardiac electrical activity acquisition. That was achieved through three bipolar leads of the frontal plane, originating the Einthoven triangle, in which the heart is located in the centre. This triangle is formed by three main points, in which the electrodes are located: right arm (R), left arm (L) and left leg (F), the connection to the earth. If two of those points are chosen, we obtain three leads in result:

- Lead I - Measures the difference of potential between the positive electrode placed on the left arm, and the negative one, on the right arm.
- Lead II - Measures the difference of potential between the right arm and left leg (positive pole).
- Lead III - Measures the difference of potential between the left arm and left

leg (positive pole).

If we move all three leads to the centre of the triangle, three intersection lines emerge, corresponding to three additional leads: aVR, aVF and aVL.

- Lead aVR - Augmented vector Right: measures the absolute potential through the positive electrode placed on the right arm (positive pole).
- Lead aVF - Augmented vector Foot: measures the absolute potential through the positive electrode placed on the left leg (positive pole).
- Lead aVL - Augmented vector Left: measures the absolute potential through the positive electrode placed on the left arm (positive pole).

With this setup, it is possible to create a division into four quadrants, knowing that when the vector is projected onto two of them (two superior quadrants), it leads to a negative deflexion on the ECG waveform, and when it is projected on the bottom half (positive half - both bottom quadrants in Figure 1.7 B), it leads to a positive deflexion. An ECG analysis typically uses more than one lead, since it allows the differentiation of artifacts (that normally don't appear in every lead), and also increasing the probability of a good acquisition and a correct diagnosis.

One important aspect that should be taken into consideration is the patient's stillness while doing an ECG exam. As this exam measures voltage potential differences in the order of millivolts, any movement will affect this signal, as it involves the use of skeletal muscles, which in turn introduces overlapping voltages that also reach the body surface. In the case where there is no movement, the exam is referred to as "Resting ECG". Also, deflexions in the ECG represent the change in electrical activity caused by atrial or ventricular depolarization and repolarization, not necessarily generalized cardiac contractions or relaxations [5].

As previously mentioned, an ECG can be obtained using different electrode locations or configurations. These can be limb leads or precordial leads (regarding locations), and unipolar, dipolar or modified bipolar (regarding configurations), respectively. In sum, there are 12 lead recording possibilities.

Up to this point, only limb leads have been mentioned: bipolar limb leads (Leads I, II and III) and unipolar limb leads (aVL, aVR and aVF). Thus, there are still 6 leads left out of the total 12. These are the precordial (or chest) ones, and measure electrical activity in the traverse plane, instead of the frontal.

In this case, the reference is in the centre of the chest and the electrodes are placed around it, as shown in Figure 1.8. The points V1 and V2 are located at the fourth

intercostal space on the right and left side of the sternum; V4 is located in the fifth intercostal space; V3 is located between the points V2 and V4; V5 is at the same horizontal level as V4; and V6 is at the same horizontal level as V4 but at the midline [3].

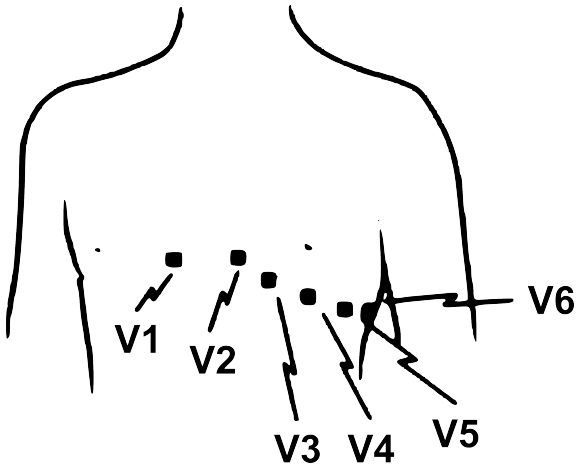

Figure 1.8: Electrode positioning for the recording of precordial leads (image adapted from [5]).

Although there are 12 possible leads for an ECG, usually not all are displayed at the same time when making a clinical evaluation. Precordial or limb leads are used according to the patient's condition and clinical interest [11]. On the other hand, using all 12 leads significantly improves the identification of cardiopathies and allows a more accurate diagnosis.

1.2 Motivation

The combination of both phonocardiogram (PCG) and electrocardiogram (ECG) exams aims to provide richer electromechanical understanding of the heart in any type of scenario, also facilitating the detection of cardiac diseases. Several devices that ally both exams have already emerged. However, the majority of them have shown limitations, preventing their standardization in medical practice.

It is also important to acknowledge that this work is part of a more omnibus project, UID/50008 SmartHeart - Smarter Cardiac Sensing via Integrated Signal Processing, in which it is intended to develop a PCG and ECG measurement device and expand it through a cloud-based machine learning toolkit, in order to extract CVD's characteristics and aid diagnosis [16], [17], [18], [19]. In the end, the idea is to create a way to easily detect a heart pathology with the help of an online database, based on a simple phonocardiogram (PCG) exam, performed in a general practice by a health-care professional. Preliminary studies performed by the SmartHeart team have lead to the choice of the 3M Littmann 3200 digital stethoscope [20] as a support tool for PCG within the project, making it a core component to this work. In particular, tests were taken in order to study performance of different stethoscopes in the detection of certain patologies. As conclusion, the Welch Allyn had the highest success, although the Littmann was one of the stethoscopes presenting the higher percentage of overall agreement [21]. However, because the latter has a native Bluetooth connectivity and does not need a wired connection to a computer, it was viewed as the better choice.

More specifically, this work intends to study a solution for ECG integration in Littmann stethoscopes, focusing also on ECG signals' segments mapping. In this way, it becomes possible to evaluate the electrical activity of the heart during a standard auscultation (PCG) exam, bringing a novel approach to a regular doctor's appointment and assisting in the diagnosis process. The importance of such practice relies on the fact that an electrocardiogram is only taken under medical prescription, while the PCG is a standard medical exam in general medicine. The main purpose of combining these two modalities is the improvement of heart disease diagnosis, as mentioned in many scientific papers in this area [22], [23], [24], [25]. Although, when used separately, the ECG and PCG may exhibit limitations in the detection of certain cardiopathies. When combined, these medical exams allow early diagnosis of heart disease. On the other hand, in countries where population has limited access to medical care, this kind of technology allows braking some barriers and facilitating

heart diseases' monitorization.

2

Background

2.1 State of the Art

The past decade has seen a great evolution in terms of devices for cardiac diagnostics. In part because of the increasing burden they have in our society, and in part because prevention is recognized as having a much bigger role than treatment itself, depending on the case and medical area, of course. In terms of stethoscope and ECG technologies, the same has happened, and devices such as the *DUO* from Eko or the *CardioSleeve* from Rijuven are now commercially available [26], [27].

DUO is a device that combines an electronic stethoscope and an electrocardiograph (1-lead ECG)[28]. It can be used with the Eko app, allowing the physician to see and review the patient's exam, as well as to share it, in a Health Insurance Portability and Accountability Act (HIPAA) compliant format, with other professionals, for a second opinion. This device provides real-time waveforms, saving and tracking possibility, as well as live streaming for use in telemedicine. It can be used in clinic, telemedicine, or at home, it is approved by the Food and Drug Administration (FDA), and it's light weight. In terms of specifications, *DUO*'s digital stethoscope has a 60x audio amplification, ambient noise reduction and 4 audio filters; the ECG system uses 2 stainless steel electrodes, a 0.01Hz high-pass filter and 500Hz sampling rate. Finally, it can be used wirelessly (Bluetooth is incorporated) to transmit data to smartphones, tablets or desktops [26], [28].

CardioSleeve is another stethoscope that provides ECG, digital auscultation and instant analysis [29]. It records four auscultation locations, using dry electrodes, and records ECG leads 1-3, transmiting the data over Bluetooth to a tablet or smartphone, and to HIPAA secure servers. In sum, *CardioSleeve* acquires ECG signals for leads I, II, and III, analyzes it, detects heart murmurs, studies the cardiac function and provides real-time tracing representation and analysis on a mobile

device [27]. Some caveats of this device are its weight (too heavy), and the mobile application used to see the medical acquisition (not fully optimized and functional).

More work has been done in this area, given rise to results such as those found in [30] and [31], which focus on developing healthcare devices that record ECG and PCG signals.

Some earlier work on PCG and ECG analysis was developed, being able to create a digital phonocardiogram that allows simultaneous ECG acquisition, combining both sound and image, visualizing auscultation and enabling the user to distinguish the location of heart sounds by ear [22]. In a more theoretical way, some studies have been more focused on the understanding of the cardiac cycle, by performing simultaneous capture of signals from multi-site auscultation with the recording of an ECG, and graphic display [23], [24].

Also, in 2014, new projects arised from the field of telemedicine [25], [32]. The work in [32] did not pass the protoptype phase, but allowed the construction of a 4-lead ECG and PCG measurement, low cost, small and wireless device. On the other hand, in [25] a new approach to pathology identification was developed, using the physical relation between PCG, ECG and photoplethysmography (PPG, also sometimes called carotid pulse). Only three volunteers were tested, two of them being healthy and one having systolic murmur due to aortic stenosis. With this, it was possible to, not only set limits to separate a normal from a pathological case in terms of peaks in the signals, but also to establish a specific time delay in the case of aortic stenosis. Thus, interconnection of all three physiological signals was also proven and demonstrated, so that heart sounds can be properly identified through ECG signals.

As frequently suggested, the accuracy of early cardiopathies detection is higher when the two major diagnosis methods are associated. By doing so, a quick preliminary diagnosis becomes possible, as well as the detection of different types of heart problems.

In conclusion, several studies have found and proved that the underpinnings of this work, combining ECG and PCG measurements, provides a more reliable and fast diagnosis [22], [23], [24], [25]. Nevertheless, existing devices are often quite cumbersome and disruptive in what concerns their form factor when compared to standard auscultation stethoscopes.

2.2 Research Goals

With this study we aim to validate and characterize ECG data acquired by means of a sensor and electrodes setup placed in the footprint of a standard diaphragm. The work spans all the constituents of the required architecture, ranging from the electrode configuration and volumetric study of the diaphragm, to the benchmarking with a medical-grade equipment, spanning also sensor design and data acquisition components. It must be confirmed that both devices acquire the same signal as the one acquired by a gold standard medical equipment.

In order to do so, two prototypes were developed and tested in several healthy subjects. Finally, similarity metrics were applied in order to determine which (if any) of the standard lead(s) better correlate with the ECG acquired from the different auscultation focuses. By doing so, it can be pinpointed which lead would a healthcare professional obtain when performing an auscultation and/or PCG exam using our devised setup.

2.3 Theoretical Basis

2.3.1 Bipolar ECG Configuration

Throughout this project, all ECG acquisitions made with the developed prototypes use a differential bipolar configuration, meaning that the electric potential is measured directly between two interest points [33]. This configuration differs from what is usually done, which involves using a third point, the reference (ground electrode). Some disadvantages may be drawn from the chosen setup, such as the short distance required between electrodes, in order to obtain a good quality signal. However, with a suitable circuit dimensioning, it still allows notorious potential difference, and plays a major role in the construction of a small, practical device, with significant impact on usability and user acceptance.

After an hefty study on the matter of electrode placement, electrode distance and signal quality [34], [35], [36], some conclusions were drawn. Not only is the distance used in this study's prototype considered adequate for a small medical device, but also there is no exact correct orientation for its placement on the chest (considering that the device is placed on the correct auscultation point), regarding both ECG and PCG acquisitions. Although the signal quality is better when putting the electrodes

aligned with the heart axis [35], [36], in general practice such specific care is not taken into account. This means that a versatile technique among professionals does not whittle down a good performance of the device. Also regarding this subjectivity, the placement of the device around the five main auscultation points, instead of the actual medical ones, has the underlying hypothesis that the resulting signal will not be significantly changed, which is one of the goals of this work.

Lastly, respecting the theoretical hurdling of the electrode placement during this study, many factors may worsen the ECG. These involve the patients' body type (more or less adiposity), physical position of the torso (supinated or pronated), psychological state (calm or nervous) and interface condition (body hair and the absence of gel), which are some of the factors that reduce the signal quality.

2.3.2 Essentials of Data Acquisition

2.3.2.1 Quantization Process and Noise

Quantization is the conversion of a continuous variable into its discrete form, in an ADC (analog-to-digital converter). For example, in a system where the signal is a voltage that varies over time (the most common approach), the voltage would be the continuous variable converted into discrete.

This process occurs in three main steps: analog input, followed by sampling, and, finally, output of the digital signal. In this way, the digital output equals the continuous input. However, at a hardware level, the process is not ideal, and, in most cases, quantization outputs are affected by the addition of a specific amount of random noise to the signal [37]. Moreover, the number of bits determines data resolution: from 10 to 12 bits, it's noticed an increase in the amplitude definition, as well as a decrease in digital noise. On the other hand, the resulting noise from this process will add to any noise already present in the original (analog) signal.

Generally, there are two limitations when digitizing a signal. First, the number of bits per sample limits the resolution of the dependent variable, meaning that small variations in the analog signal may go by unnoticed (certain different values of the analog signal will have the same value assigned by the quantizer). Second, the sampling frequency itself limits the resolution of the independent variable, meaning that closely spaced events may also go by unnoticed.

In this study, when using a 10 bit sensor, to measure ECG signals, in the range ±

1.5mV, both the gain, full scale voltage of the ADC, and the number of bits will affect the resulting digital signal. Therefore, input values can assume 1024 (2^{10}) different values, 0 corresponding to 0V, and 1023 (1024-1) corresponding to 3.3V, according to the sensor specifications. On the other hand, the input range gives place to the mentioned output range due to the gain factor and reference voltage of $1.65V$.

2.3.2.2 Sampling Frequency and the Nyquist Theorem

Proper sampling happens when one can extract a minimal amount of descriptors that enable the reconstruction of the analog signal from the samples, while these provide an adequate representation of the analog signal itself [37]. On the other hand, improper sampling means that the signal may have its frequency content masqued; this is called aliasing. The samples would represent a wave different from the one contained in the analog signal [37]. From this rises the Nyquist-Shannon theorem, which establishes that: "(...) a continuous signal can be properly sampled, only if it does not contain frequency components above one-half of the sampling rate." (from [37], in "The Sampling Theorem"), meaning that the relation $f_s > 2 \times f_{max}$ needs to be guaranteed by the whole sampling system. When this inequality is not respected, the frequencies above the limit will be masked and combine with the original information already there, resulting in a new, unreal, signal, upon reconstruction. As an example, with a 4kHz signal, the sampling frequency should be greater than $2 \times 4\text{kHz} = 8000$ samples/sec, in order to avoid signal disruption.

2.3.3 From the Physical Process to a Digital Representation

From the physiological process itself to the digitized ECG signal, different steps are involved. This process is schematically represented below (Figure 2.1) and it's based on [38].

- Electrodes - When placed over the skin, the electrode contacts with the electrolyte (gel or paste to increase skin conduction), and ion-electron exchange occurs, resulting in the the half-cell potential, *i.e*, a characteristic potential difference established by the electrode and its surrounding electrolyte [33], [39]. Also, due to the skin-electrode contact, there is always ion accumulation between the two, making it more difficult to measure an ECG signal. This

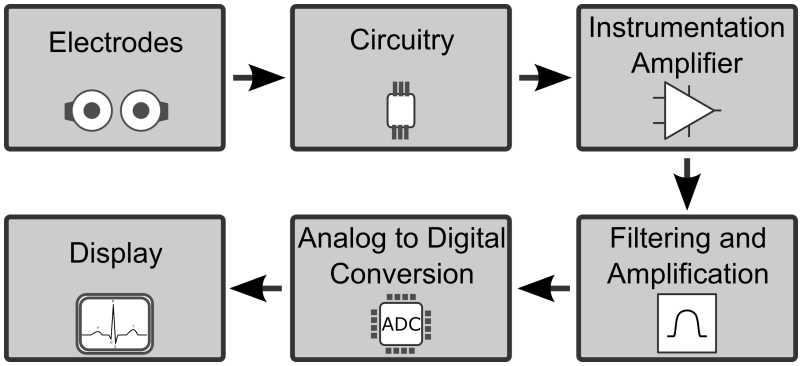

Figure 2.1: Schematic representation of digitization process.

way, it is important that the sensor can overcome this problem, by having a good amplification component, for example. When talking about the type of electrodes, these should be good conductors and provide limited offset and low noise. One example of a good and commonly used option for ECG electrodes is Ag/AgCl. Another detail to consider is the protection of the connecting cable from possible electromagnetic noise sources.

- Instrumentation amplifier - This is the element responsible for making sure that the physiological signal amplitude is scaled to reach the range of the sampling circuitry, since an ECG usually is around a few millivolts, and the ADC is prepared for signals around volts. Therefore, some sort of amplification is needed.
- Analog to digital converter (ADC) - As previously described in Section 2.3.2.1, is the component responsible for converting an analog signal into a computationally manageable digital representation; the higher the resolution, the higher the amplitude definition of the signal in the digital domain.
- Filtering and second-stage amplification - Filtering wise, the process must be very meticulous, given that ECG sensing can be affected by cross-talk from other muscles, AC power, and radio-frequency interference, that can mask the signal of interest.

3

Support Tools

3.1 Starting Point

Throughout the entire project, the chosen platform for electrocardiogram signal acquisition was BITalino [40], [41], motivated by the fact that schematics are freely available, the platform has seen extensive validation in previous work, [40], [42], and the modification of the circuitry specification to meet unknown aspects anticipated within the work is fairly manageable without external dependencies. From there on, numerous prototypes were developed, taking into account the findings resulting from the multiple experimental stages of the work, in order to evolve up to a point where a high performance, practical and ergonomic sensor configuration was devised.

BITalino is a hardware and software toolkit that has been specifically designed to deal with the requirements of body signals. In this specific case, it was used to measure ECG signals in a more practical and cable-free manner, since it can communicate through Bluetooth.

The starting point was a BITalino version with a sampling frequency of 1000Hz and an amplification gain of 1100. From that point forward, some modifications took place, adjusting the analog frontend to a variant more suitable to the work at hands.

Specifications of the already modified ECG sensor are presented in Table 3.1, where one can also find features regarding the original BITalino device. The modified version developed in the scope of this work, includes a more extensive set of changes (see Figure 4.1), for which a detailed description is provided in Section 4.1.

As described in Section 1.2, the goal of this work is to integrate ECG sensing in a standard stethoscope form factor, in particular the diaphragm. This poses several constraints such as the electrode geometry (to prevent masking the PCG signal), the inter-electrode spacing (due to the limited real estate in the diaphragm), and others that affect, for example, the signal amplitude, in ways that were pre-

Table 3.1: Specifications of the ECG sensor.

Specification	**Original**	**Modified version**
Measurement range	± 1.5mV	±.33mV
Bandpass Filtering	0.5-40Hz	
Input Impedance	> 1MOhm	
CMRR	110dB	
Gain	1100	5600

viously unknown. Preliminary tests have revealed that the standard configuration of the BITalino hardware base did not suffice, in particular the signal amplitude that was experimentally found to be almost one order of magnitude lower than that for which BITalino has been designed (see Section 4.1.3), and several modifications were needed.

The transfer function of this new ECG sensor is given by Equation 3.1. The ADC value is the value sampled from the channel; 2^n is 1024 for the BITalino channels (given the 10-bit resolution); VCC (the operating voltage) is 3.3V and the denominator is the ECG gain (gain of the instrumentation amplifier multiplied by the gain applied after filtering), in our case 1100 or 5600, depending on the device (more details in section 4.1.3). The latter gain value allows the setup to measure ECG signals with a dynamic range of $[-0.33mV, 0.33mV]$, which was empirically determined from preliminary tests performed with the standard setup.

$$V_{ECG} = \frac{(\frac{ADC}{2^n} - \frac{1}{2}) \times VCC}{G} \tag{3.1}$$

As mentioned, raw ECG signals were acquired with a customized version of BITalino, used in a 10 bit resolution and 1kHz sampling frequency configuration. Table 3.2 describes the main specifications of the biosignal acquisition unit.

Considering the goal of this work, focused on integrating ECG sensing in the footprint of a standard stethoscope diaphragm, we developed a hardware simulator, considering such requirement, as a way of supporting the experimental part of the work. Taking into account the standard auscultation process, a circular, stethoscope-like diaphragm form factor was developed.

Table 3.2: Specifications of the BITalino device.

Specification	Value
Connectivity	Class II Bluetooth Connectivity
Wireless Range	up to 10m
Resolution	up to 10-bit
Sampling Rate	up to 1000Hz
Weight	74g
Size	84mm×53mm×18mm
Battery	Li-Po; 7.4V; 500mAh

3.2 GE Healthcare MAC 800 Resting ECG

This electrocardiograph was used as gold standard, in order to validate the prototypes' performance and support the experimental part of the work. Some important features are highlighted in Table 3.3.

The MAC 800 electrocardiograph is a portable and accurate system that allows storing, archiving and editing of previously recorded ECG waveforms. It has multiple communication options, such as LAN, modem, SD card and serial port, and has two memory options, up to 100 ECG records stored internally, and SD card export for analysis in external tools.

It is highly accurate and provides several ECG analysis programs that enhance diagnostic confidence. It provides immediate visualization of the records, but also their printing for further in-depth analysis [43].

3.3 3M Littmann 3200 Digital Stethoscope

As previously mentioned, the gold standard for heart sounds used in this project was the 3M Littmann 3200 digital stethoscope. Its main specifications are presented in Table 3.4. It has an amplification of 24x and a band-pass filter that can be setup in three different modes, emphasizing specific frequencies (see Table 3.5).

The choice to use this specific digital stethoscope was made by the group working on the SmartHeart project, after consideration of all digital devices available. Not only the evaluation of sound quality was taken into account by a cardiopneumologist, but also the type of connectivity was thought of as well. As the 3M Littmann

Table 3.3: Specifications of the GE Healthcare MAC 800 electrocardiograph (used as gold standard).

Specifications	**Description**
Instrument Type	Microprocessor augmented automatic electrocardiograph 10-leadwire 12-lead simultaneous acquisition with programmable lead configuration
Sampling Frequency	500Hz
Acquisition Mode	Provides 10 seconds ECG strip (export to SD card in XML)
Dynamic Range	AC differential $\pm 10mV$, DC offset $\pm 300mV$
CMRR	>90dB
Input Impedance	>10MΩ

Table 3.4: Specifications of the 3M Littmann 3200 digital stethoscope.

Specification	**Value**
Diaphragm Diameter	5,08cm
Diaphragm Material	Polyurethane-coated silicone
Length	68,58cm
Net Weight	185g

Table 3.5: Filter options available on the 3M Littmann 3200 digital stethoscope.

Mode	**Range of Amplification**	**Emphasized Frequencies**
Bellmode	20-1000Hz	20-200Hz
Diaphragm	20-20000Hz	100-500Hz
Extended Range	20-20000Hz	50-500Hz

Figure 3.1: GE Healthcare MAC 800 Resting ECG acquisition setup.

3200 digital stethoscope has a native Bluetooth interface and does not need cabled connection to a computer, this device was viewed as the better choice [21].

As such, the 3M Littmann stethoscope was then used as a guideline for the auscultation sounds recorded.

3.4 BITalino R-IoT

BITalino R-IoT is an association of a BITalino sensor (with a lower sampling frequency) and a router that manages the WiFi connection with a computer (Table 3.6).

This device was chosen due to the influence that spatial and planar rotation has in ECG signals. When performing an auscultation, the healthcare professional does not have a strict way of placing the stethoscope, as long as it is on the right focus, since its rotation does not alter the PCG signal. However, when acquiring ECG, this same placement freedom of the device will lead to different signals, with different polarities, due to the position change relatively to the heart's axis.

As such, by using the R-IoT sensor, one can study the rotation angle that the stethoscope suffered, and thus, study how this specifically influences the ECG.

Figure 3.2: 3M Littmann 3200 digital stethoscope (promotional image).

Table 3.6: Specifications of the R-IoT device.

Specification	**Value**
Connectivity	WiFi 2.4GHz
Sampling Rate	200Hz
ADC Voltage	1.8mV
Working Voltage	3.3V
Resolution	12-bit
Size	34mm×24mm×2.5mm

3.5 Python for Scientific Computing

In order to perform such previous signal analysis, Spyder (a Python Integrated Development Environment) was used.

Anaconda 4.4 was the chosen Python (version 2.7) distribution to perform data analysis. The main libraries used were Matplotlib, SciPy and NumPy.

Scipy is a Python-based ecosystem of open-source software for mathematics, science, and engineering. It contains packages such as NumPy, IPython, SciPy library, Sympy, Matplotlib and pandas. Throughout this project, NumPy and Matplotlib were the core of our data processing.

NumPy is a package for scientific computing in Python, providing facilities such as

efficient vector and matrix data representation and operations, including dimensionality manipulation, sorting, slicing, application of logical and mathematical operators, amongst many other convenient features.

Matplotlib is an advanced plotting library for Python, with a wide array of display options and exporting capabilities. In the scope of this work it has been primarily used for bidimensional data plotting, visualisation and automated exporting of the figures in a suitable format.

4

Implementation

4.1 Stethoscope Sensor Mounting Simulator

As it was required to register both ECG and PCG signals, a first prototype was developed (see Figure 4.1).

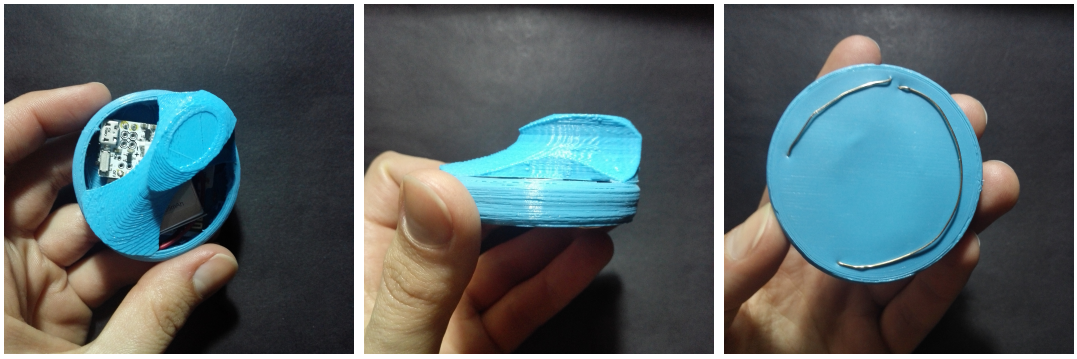

Figure 4.1: SmartHeart prototype device. Figure 4.1(a) Top view of the hardware simulator with the battery, acquisition and communication electronics inside; Figure 4.1(b) Side view of the device showing the grip used to apply the simulator to the device; Figure 4.1(c) Bottom view of the device showing the electrodes configuration.

For that, a BITalino sensor was incorporated in a thermoplastic polyurethane (TPU) diaphragm, printed in a desktop 3D printer. This TPU membrane intended to simulate the real membrane used in the 3M Littmann Digital Stethoscopes [44], our PCG signal reference device (due to its native Bluetooth support for wireless connection to a computer). This was a crucial step to study the mechanical integration of the ECG sensor, given that the standard diaphragm covers do not have space to accommodate additional components. Inside the diaphragm were a 110mAh lithium-polymer (LiPo) battery, an ECG sensor, the BITalino data acquisition hardware base and, attached to the outside surface, was a pair of AuAgPl (80% gold and 20% silver and platinum) alloy electrodes.

4.1.1 Diaphragm Models

To support the validation work and prototype construction, a model was developed with OpenSCAD, as seen in Figure 4.2.

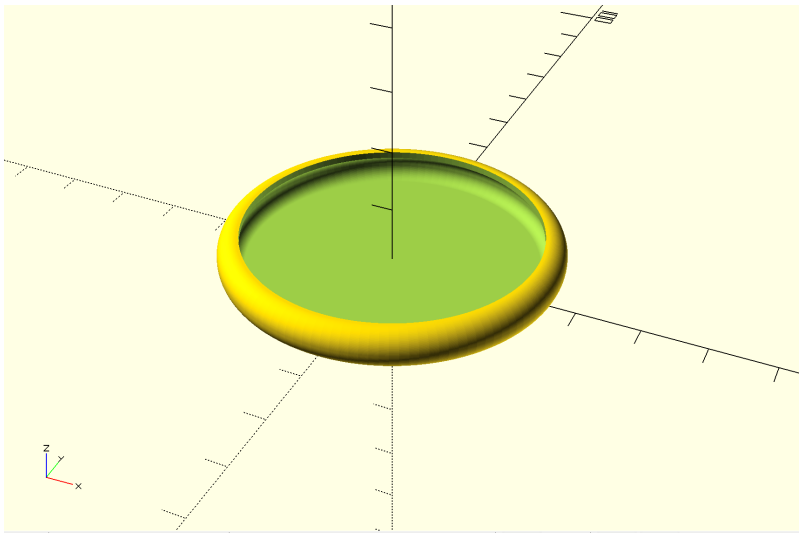

Figure 4.2: Diaphragm model developed with OpenSCAD.

Since the standard structure of the stethoscope didn't allow the incorporation of the additional elements (see Figure 4.3, number 187), it was beneficial the development of a new membrane design, and this way avoiding damaging the original piece. By resorting to an unattached diaphragm, we were able to freely and agilely test different geometries. Another aspect of this model was the study that a cavity in the membrane would have in the stethoscope's performance, and how one could develop a shape that minimized its influence.

4.1.2 Electrode Dimensioning

For this type of setup, the typical Ag/AgCl electrodes were not used because their physical charateristics and geometry do not allow proper moulding and adaptation to the specific mechanical characteristics of the 3M Littmann stethoscope, without interfering with the usability of the device and performance of the PCG signal acquisition component [45].

Gold electrodes can be separated from Ag/AgCl ones due to their polarization properties. The firsts (gold) are polarizable electrodes (meaning that no charge crosses the electrode when current is applied), are difficult to oxidize and dissolve, and behave like a capacitor. They can be used to record biopotentials, but in general are

better suited for higher frequency biopotential measurements [33]. With this, gold electrodes are not the first choice for measuring ECG signals, but rather Ag/AgCl. On the other hand, the latter are non-polarizable. As so, they behave resistively, are better suited for biopotential recordings that range from high frequency to very low frequency, and, therefore, are usually the best choice for ECG exams [33].

Nevertheless, gold has been shown to have good performance when used for measuring biopotentials, including electrocardiography signals ([46], [47]), and meet the standards for our particular application: high conductivity, easy to mould into the shapes found suitable for this study, and possible to obtain in a miniaturized size, this being an important feature for the integration of this part of the setup on the diaphragm. Not to mention that gold is considered a reference material for some biosignals measurements.

Therefore, this kind of assembly favours the combined acquisition of both ECG and PCG signals.

4.1.3 Sensor Dimensioning Targeting a New Prototype

Not only the diaphragm structure had to be studied, but also the performance of BITalino sensor (with the standard specifications) needed to be tested when incorporated in this type of assembly.

Regarding the membrane, three versions were considered. Between a deep hollow version, a version with a TPU solid filled center (in the position where the acoustic sensor is mounted on the stethoscope), and a version that exactly resembled the original, the chosen was the second (model 191 in Figure 4.3). The design of the three alternative diaphragms intended to assure different aspects of the setup. The hollow model with a hard nucleus in the center (second and third from the left in Figure 4.3) was meant to study how the sound was best heard, comparing to the hollow center deep membrane (first from the left in Figure 4.3), which was an attempt to allow all electronic elements to be inside it, making the stethoscope much more practical. And, finally, the thin, completely hollow model (fourth from the left in Figure 4.3), which most resembled the original one, was designed to assess if the difference in materials with which the membrane is produced affects the performance of the diaphragm.

More model variations were tested, with different heights of the central core. Figure 4.3 shows a photograph of all membranes designed for this project, along with the

original 3M Littmann diaphragm cover (in black), as well as a 3D printed counterpart using rigid material (in white). From right to left, we have the original 3M Littmann cover (187), the rigid poly(lactic acid) (PLA) transparent cover (188) and four flexible Thermoplastic Polyurethane (TPU) versions (depicted in blue): completely hollow model, replica of the original (189); hollow model with a 2mm hard core in the center (190); hollow model with a 4mm hard core in the center, deeper than the previous (191); and a filled model with an empty nucleus (192).

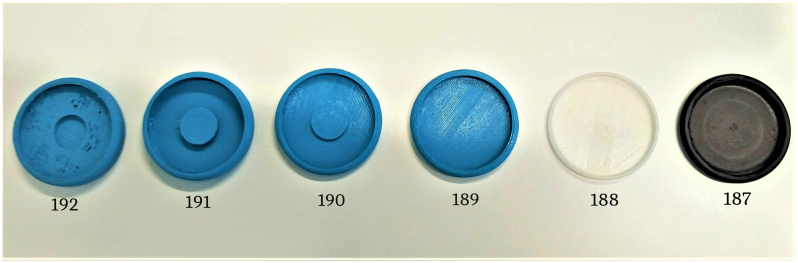

Figure 4.3: Line-up of all six tested diaphragm models.

The membranes were tested by three evaluators (two professionals and one non professional) whom listened to several heart sounds using a randomly chosen diaphragm, out of the six already mentioned. This process was done without the evaluators knowing what membrane they were using, and the fact that an amateur was involved in the experiment intended to add a sensitivity variable to it (this evaluator is more sensible to noise). A total of 12 cases were studied, and each criteria was scored by the evaluators on a five-point scale.

Regarding the first four parameters (ability to hear heart sounds S1/S2; breathing; device noise; external noise), number 1 stands for "Nothing heard", number 2 means "Heard sometimes", 3 means "Slightly heard", 4 means "Audible", and 5 means "Pretty well heard".

On the other hand, the Noise *vs.* Heart Sounds criteria was evaluated from one to five, having the following meaning: 1 - "Only noise is heard"; 2 - "Mostly noise"; 3 - "A little bit of both is heard"; 4 - "Mostly heart" and 5 - "Only heart is heard".

Finally, the General classification of a membrane can be 1 - "Not good to identify heart sounds", 2 - "Gives some information", 3 - "Allows identification after a while (needs ear training)", 4 - "Allows identification by a professional", and 5 - "Allows identification by a medical student".

The results are presented in Table 4.1, according to the previous scales. It must be taken into consideration that the evaluators used the same diaphragm twice, and,

Table 4.1: Custom diaphragms evaluation summary.

Specification	**Model**					
	187	**188**	**189**	**190**	**191**	**192**
S1/S2	3.83(3)	4.167	4	3	3.667	2.667
Breathing	1.83(3)	1.667	1.83(3)	1.167	1	1
Noise	3.33(3)	4	4	2.667	3	3
External noise	1.83(3)	1	1.83(3)	1.667	1.167	3.83(3)
Noise *vs.* heart sounds	3.50	3.33(3)	3.167	3	3.50	2.33(3)
General	3.83(3)	4	4	2.667	3.83(3)	2.167

for better understanding of the collected data, the table below presents the mean of the score assigned to each model.

From the General evaluation values, it can be acknowledged that the best classified diaphragms were the rigid PLA (transparent) model (188) and the flexible TPU most similar to the original model (189). Heart sounds are best heard, but the noise created by the device is amplified as well. When considering the Noise vs. Heart Sounds criteria, model 191 performed better. For the rest of the diaphragms, they not only reduce the noise, but also muffle the sound. Likewise, one can also verify that the 191 model showed a similar over-all performance comparing to the original version (187). Considering its classification and depth (which allowed the integration of all electrical components), the 191 model was chosen.

This analysis is purely subjective and, after examining for a while, the evaluator himself is more responsive and identifies more easily the sounds. In any case, this part of the work follows the procedure previously set forth by the SmartHeart team in [21].

Meanwhile, the total assembly of the sensor (SmartHeart prototype) was also tested. When compared to a Lead-I BITalino typical device, SmartHeart revealed low signal magnitude. This experimental test involved two different setups. The first one was an ECG-first-Einthoven-lead acquisition, with the negative electrode on the right clavicle, the positive one on the left clavicle, and the ground placed on the left lower side of the trunk. The second setup involved acquiring ECGs in all five PCG focuses with the membrane and SmartHeart prototype. In this last case, the auscultation points were the second intercostal space on the right parasternal line, the second intercostal space in the left parasternal line, the third intercostal space in the left parasternal line, the lower left border of the sternum and the fourth/fifth intercostal space in the left hemiclavicular line (see Figure 1.1).

Table 4.2: Preliminary measurements obtained for an Einthoven triangle sensor placement.

Metric	**Value**
Mean of R-peaks	0.1065 mV±0.0421
Mean of minimum peaks	-0.0747 mV±0.0382

Table 4.3: Preliminary measurements obtained with the hardware simulator.

Metrics	**Values**					
	F1	F2	F3	F4	F5	Global
Mean of R-peaks	0.0339mV	0.0408mV	0.0427mV	0.0403mV	0.1539mV	0.0544mV
Standard deviation of R-peaks	0.0070	0.0075	0.0104	0.0386	0.2417	0.0973
Mean of min. peaks	-0.0451mV	-0.0414mV	-0.0349mV	-0.0575mV	-0.1123mV	-0.0535mV
Standard deviation of min. peaks	0.0077	0.0087	0.0051	0.0104	0.0863	0.0400

Results are presented in Table 4.2 & 4.3. Figures 4.4 & 4.5 show small segments of the acquired signals, as well as the overlap of each auscultation focuses' templates (*i.e* heart beat waveform).

It can be observed from the acquired data that ECG values from the Einthoven setup usually go up to approximately 0.11mV, while ECG values measured with the diaphragm only reach about 0.04mV; as such, the gain of the sensor was found to be extremely low when considering the dynamic range of the ADC, motivating the need to modify the analog frontend of the sensor, and thus creating a new prototype, so that its sensitivity can be more adapted to the chosen setup.

As described in Section 3.2, 5600 was the estimated gain value for the second prototype (more details ahead, in Section 4.2), based on empirical evidence, and further confirmed by the experimental component of the work. This way, the electrocardiogram signal amplitude is around ±0.33mV. We believe that this is consequence of the reduced inter-electrode distance imposed by the small footprint of the diaphragm, which results in a lower voltage potential difference between the IN+ and IN- inputs of the amplifiers (see Section 5.2.5 for additional details).

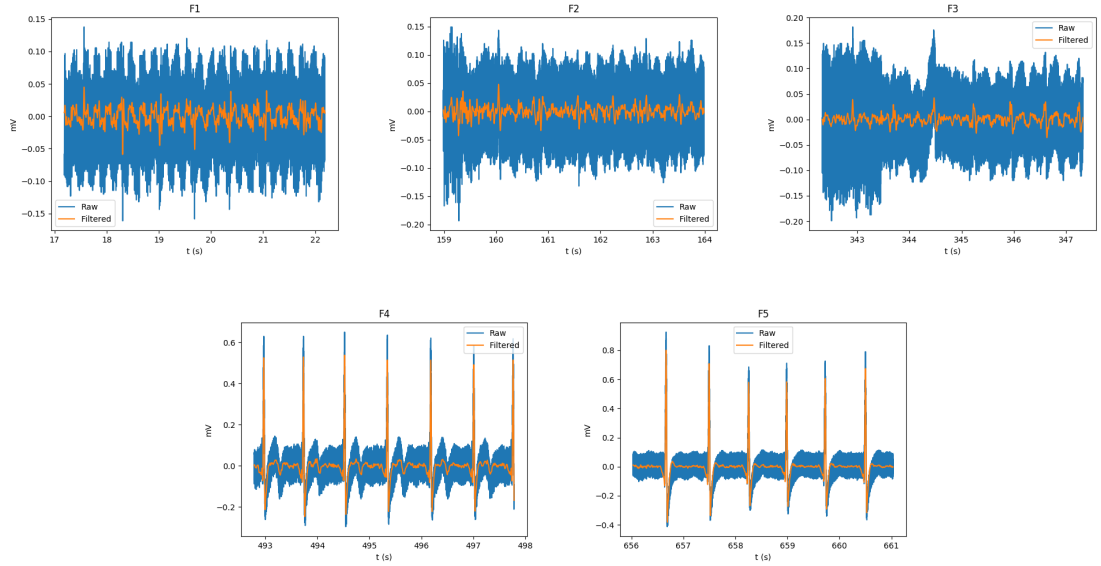

Figure 4.4: Short time segments of the acquired ECG on the auscultation points with the diaphragm setup (focuses F1 to F5 represent the five main anatomical auscultation points).

4.2 Accounting for Placement with Respect to the Heart Electrical Axis

A different configuration of the system was taken into account, in order to evaluate whether (and how) the positioning angle during the auscultation exam influenced the resulting signal. For this purpose, a BITalino R-IoT device was used (herein after designated as R-IoT), since this specific configuration has an onboard inertial measurement unit (IMU), contrary to the remaining, allowing the measurement of the diaphragm's angle in space, with respect to the earth's magnetic pole.

For this prototype, a similar approach was made. A diaphragm was printed and a R-IoT board, as well as an ECG sensor and a lithium polymer battery, were assembled inside. This version differs from the previous not only on the measured signals (this one has the ability to measure the rotation angle of the stethoscope), but also in the sensor features, given that the ADC has a lower input range (see Table 3.6), and the chosen gain (5600) was already more suitable to the signals acquired. Figure 4.6 depicts the implemented prototype.

Also with a lower sampling frequency, the R-IoT device was a compromise between angle measurement and ECG measurement. Furthermore, a switch was added to enable the examiner to mark where a good signal begins to be acquired, and when the

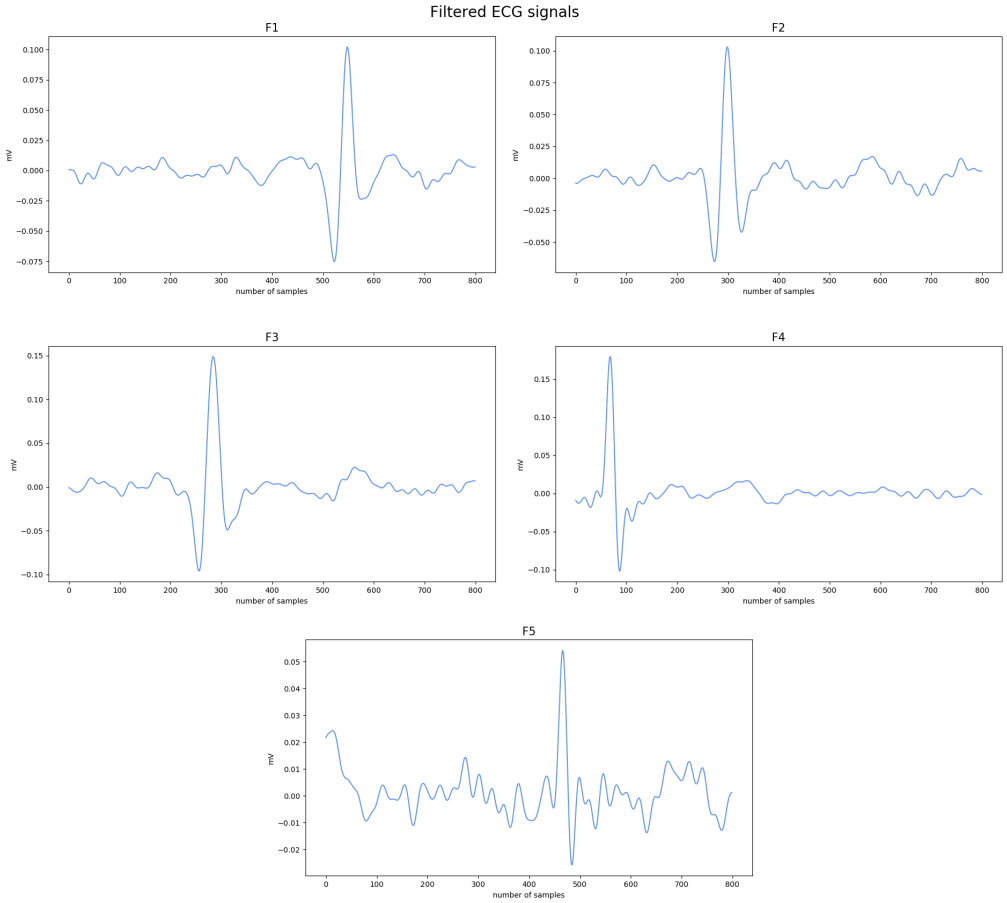

Figure 4.5: Representation of each acquired ECG templates for focuses F1 to F5, with the diaphragm setup.

portion of quality acquisition ends. To assemble this switch, two resistors (valued 1kΩ and 1.2kΩ) had to be mounted on the BITalino R-IoT board to match the output voltage on the switch to the input voltage of the ADC. The combination of both adds an additional channel, indicating when the switch is turned on or off, through a square wave, seen in an appropriate visualization platform.

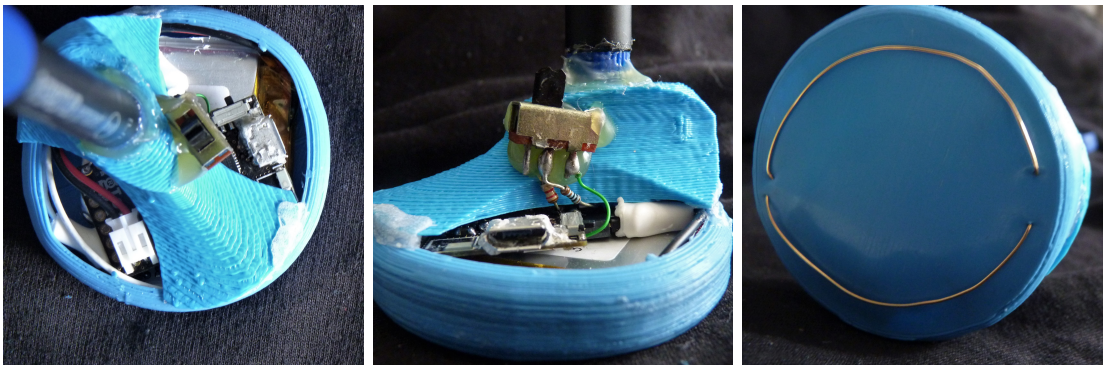

Figure 4.6: R-IoT prototype device. Figure 4.6(a) Top view of the hardware simulator with the battery, acquisition and communication electronics inside; Figure 4.6(b) Side view of the device showing the grip used to apply the simulator to the device; Figure 4.6(c) Bottom view of the device showing the electrodes configuration.

5

Methods

5.1 Experimental Protocol

After the development of the two hardware simulators, namely the SmartHeart device and the BITalino R-IoT, we focused on testing them against a medical-grade gold standard, with the goal of evaluating their performances. Whilst the standard 12 leads and electrode placements used in regular practice are fully characterized in literature, the setup devised in the scope of this work has several properties that make it significantly different from both the standard 12 lead ECG (see Chapter 4) and from other approaches found in the state of the art (see Section 2.1).

To do this, several acquisitions were intended to be performed at a medical facility. However, due to the heavy workload and overall busyness of the institution, the initial plan was rearranged. As such, for the experimental data acquisition, only healthy subjects were evaluated, under the guidance of a cardiopneumologist, and the used gold standard device was the MAC 800 [43], from GE.

This setup consisted of GE MAC 800, SmartHeart stethoscope simulator and R-IoT device. Preliminary tests were initially performed on two subjects, so that adjustments could be made in terms of data processing, electrodes positioning and overall setup details.

With the gold standard all twelve leads were acquired, while with the SmartHeart device ECG signals were collected in all five auscultation points, one at a time, with random orientations of the diaphragm (positioning was done according to personal preference). With the R-IoT all five auscultation points were evaluated, one at a time, this time with ninety degree angle variations between each position, for each focus.

All this information is further detailed in the appendices section (see section A.1).

5.2 Experimental Analysis

5.2.1 Data Processing

Throughout this project, comparison of the signals acquired with the developed prototypes and a gold standard device was a central point. From filtering, to the R-peak detection within each ECG segment, to the segment selection itself, and to the instant heart rate calculation, the BioSPPy toolbox[1] [48] was used as a support tool.

Within this toolbox, the module *ecg.py* contains a set of functions for feature extraction and segmentation, which were used to support the pre-processing component of the work. In terms of filtering, it uses a bandpass finite impulse response (FIR) with order corresponding to 30% of the sampling rate, this being identified as a suitable approach in previous work by the group. For R-peak location and extraction, an ECG R-peak segmentation algorithm is used, following the approach by [49].

For the heartbeat waveforms (herein also designated templates), which are a segment of the signal in time, corresponding to a heart beat cycle, a criteria that selects 0.2s before the R peak and 0.4s after is used, taking into account the known physiological time intervals for a heart rate at rest. For heart rate calculation, the used module extracts heartbeat templates from an ECG signal, given a list of R-peak locations.

The analysis algorithms were divided into three SmartHeart scripts, three R-IoT scripts, and two for MAC 800 gold standard device. The main script would receive inputs such as the name of the subject in study and the index values that limited the segment of interest in each evaluated signal. The remaining files would be responsible for getting the sensor's channel with the ECG data from each device, convert it to millivolt (its correct physical units) and extract the main portions of signal that represent each quality segment, based solely on the visual inspection and annotation (F1, F2, F3, F4 & F5 for the SmartHeart device; and positions 90, 0, -90, -180 for each focus, for the R-IoT device). Moreover, filtering, feature extraction (such as the templates and R-peaks), mean waves calculation, MAC 800 signal interpolation, performance metrics calculation (Euclidean distance, coefficient of determination and root mean square error) and compilation of the results to an Excel spreadsheet were performed on the main script.

As stated above, when running this program, one has to identify which portion of

[1] https://github.com/PIA-Group/BioSPPy

the already limited signal is of interest and presents the lowest noise amplitude. This allows better control of what goes into the processing workflow, avoiding extremely noisy signals to be processed.

5.2.2 Preliminary Studies

In order to study the first setup of electrodes (see Section 4.1.2), a preliminary characterization was performed. This involved the determination of statistical parameters such as interpolation, synchronization, root mean square error and coefficient of determination.

This study was conducted in order to gain a better understanding of both the SmartHeart and R-IoT prototypes, by using a gold standard device as reference.

Before the actual experimental study with ECG signals from a large number of subjects, several preliminary studies of this type of data were taken into account, in order to test the setup and identify potential improvement points. This has been crucial for the development of the prototypes, and to reach the final integrated version that resulted from this work.

As previously described, in the scope of our work we used as gold standard the GE MAC 800 device [43]. However, this device introduced several constraints and difficulties to the work. Not only the sampling frequency was significantly different amongst devices (1000Hz for the SmartHeart, 200Hz for the R-IoT and 500 for the MAC 800), but the recording conditions were also limited. In order to minimize the effect of the different sampling rates, we interpolated the signals acquired with lower sampling rate to match the highest sampling rate, so that all signals could be more adequately compared. Moreover, when using this gold standard, only 10 seconds of data were possible to export in digital format (the maximum time span allowed by the device for export), using a XML structure that is poorly described and supported in common programming languages.

To make this part of the work clearer, some definitions are given below.

- Interpolation: As the acquired signals did not have the same sampling frequency, there was the need to make them more comparable; in our case, instead of sub-sampling the signal acquired with higher frequency (hence loosing time resolution), we chose to perform linear interpolation of the signals acquired using lower frequency, which consists of upsampling.

- Synchronization: To analyse the morphological similarity of the signals, a crucial aspect is the precise temporal alignment, and, due to the lack of suitable input channels to do so on the GE MAC 800, synchronization of the recordings was performed by cross-correlation of the time series; cross-correlation can only be performed between signals that have the same sampling rate, further reinforcing the importance of the previously described interpolation step.
- Root mean square error (RMSE): RMSE is the standard deviation of prediction errors. It can show how concentrated the data is, around the line of best fit. In this case, as the goal is to compare different sets of data (mostly from two different devices: MAC 800 *vs.* SmartHeart and MAC 800 *vs.* R-IoT), the RMSE is used as a dissimilarity metric, albeit possessing limitations to be used by itself; in particular, scaling of the signals can be an issue, reason for which we found a need to normalize it, in order to obtain relative values and be able to compare signals.
- Coefficient of determination (R^2): This value evaluates the quality of linear regression applied to the data; the bigger the value, the better the fit between two data series is.

Several tests were performed regarding the signal synchronization. Initially, an all signal analysis was attempted, by considering all points of some ECG features, such as QRS complexes and heart rate. However, this approach failed, as some of the peaks weren't exactly aligned, due to missing data and noisy portions of the signal trace. With that, synchronization was then tried, by using the heart rate (bpm) from each signal, *i.e*, by performing a wave morphology study. By using the BioSPPy toolbox, it is possible to obtain the delay between two signals. The idea was to use this delay to identify the portion of SmartHeart and R-IoT signal where the heart rate correlation to MAC 800 was higher, and therefore, segmenting the window of interest in the SmartHeart and R-IoT data.

In terms of statistical analysis, RMSE and coefficient of determination functions also had to be tested. These tests were performed by initially using two square waves, one much longer than the other, but with the same number of total samples. The point was to create a sliding window and look for the shorter segment within the other. When matching was obtained, R^2 equalled its maximum value, 1. The Euclidean distance was also measured. This specific experiment intended to replicate the already seen delays when performing a synchronized ECG acquisition with MAC 800 and BITalino systems. These delays, however, are created by the natural operation workflow, in the sense that in a single person acquisition scenario, it is difficult to

start both devices at the exact same time.

5.2.3 Auscultation Learning and Littmann Synchronization

Considering the final goal of integrating ECG data acquisition in the device used for PCG, the problem of data synchronization is once again evident. In particular, we have two independent devices acquiring the data of interest (our prototypes and the stethoscope), which, without a suitable common reference signal, constitutes a problem in post-processing. To address this problem, a preliminary PCG-ECG synchronization study was performed, with the SmartHeart project team from Porto.

A 3M Littmann 3200 stethoscope and a SmartHeart prototype variant were used, with the latter including a user-controllable buzzer. This enables the injection of a known acoustic signal in the PCG data, with the triggering event being marked in the SmartHeart prototype. Being a common event to both systems, it can be used in post-processing to automatically determine the point where it happened in each time series, and align both by removing the temporal offset preceding the event.

While a cardiopneumologist acquired phonocardiogram signals from the five main auscultation points on a person holding an earlier iteration of the SmartHeart prototype (collecting data on a single focus), data was collected using the OpenSignals (r)evolution software[2], through which the buzzer was manually triggered whenever the professional reported a good sound.

Also, during this session, we were taught how to perform an auscultation exam according to a professional's technique, in order to be able to accurately replicate the process in the experimental part of this work.

5.2.4 Signal Amplitude Characterization

After testing the R-IoT configuration, saturation was quickly noticed in both auscultation points four and five (F4 and F5, respectively).

With this, a possible solution approach was though of; for points F1, F2 & F3 (the first three described in section 4.2) calculations were made in order to estimate how higher the setup gain should be, since these focuses remark to the farthest points from the heart and presented low amplitude signals with the initial system; while for points F4 & F5, which were usually of much higher amplitude than the latter,

[2]http://bitalino.com/en/software

Table 5.1: Estimated gains for focuses F1, F2 and F3.

F1		**F2**		**F3**	
Max peak	$\hat{G}$	Max peak	$\hat{G}$	Max peak	$\hat{G}$
0.052mV	17307.69	0.0767mV	11743.03	0.1287mV	6993.00

given the heart proximity, calculations were made in the sense of ascertaining how lower the gain could be. In sum, this aimed the study of the most suitable gain for each set of focuses (F1, F2 & F3 and F4 & F5), in order to have a good quality signal.

For the first set of focuses (F1, F2 & F3), this was done by assessing the higher signal amplitude (corresponding to the R-peak), for the referred three focus. With that, the sensor gain was estimated, based on the idea that the ECG signal is centred in $\frac{V_{CC}}{2}$, and so, its amplitude must be multiplied by a certain gain, in order to achieve the intended value (Equation 5.1). Results can be seen in Table 5.1.

$$R_{max} \times G = \frac{V_{CC}}{2} \tag{5.1}$$

$$\hat{G} = \frac{VCC}{2 \times R_{max}} \tag{5.2}$$

On the other hand, for points F4 & F5 (the remaining mentioned in section 4.2) R-peaks amplitudes, as well as the lowest peaks, were interpolated to obtain an estimation of the maximum amplitude values, since the saturation did not allow empirical identification of the R-peak value. For this, segmentation of F4 and F5 acquisitions was necessary (see Table B.1 in appendix, x_s being the beginning and x_e being the end of each segment). Similarly, after assessing the range of the ECG signal, gain was estimated based on Equation 5.1.

In Tables 5.2 & 5.3 both saturated values before interpolation and estimated values after interpolation, are presented, resulting in the corresponding gains in Table 5.4.

Based on the analysis of each data set, it was concluded that the most appropriate gain for focuses F1, F2 & F3 was approximately 6500, and for F4 & F5, it would be approximately 6000. Although the difference might not be outstanding, it is enough to avoid saturation of signals acquired in focuses F4 and F5. Nevertheless, the main conclusion is that the sensor needs to have an adjustable gain in order to have the best performance, given the disparity of amplification gains required in-between focuses.

Table 5.2: Saturated values of R peaks for both focuses F4 and F5.

Position	**Values (mV)**			
	F4		**F5**	
90º	max	0.1276	max	0.1265
0º	max	0.1283	max	0.1269
-90º	max	0.1282	inverted R-peak	-0.0764
-180º	max	0.0997	inverted R-peak	-0.0821

Table 5.3: Interpolated values of R peaks for both focuses F4 and F5.

Position	**Values (mV)**			
	F4		**F5**	
90º	max	0.1371	max	0.1322
0º	max	0.1332	max	0.1393
-90º	max	0.1485	inverted R-peak	-0.0794
-180º	max	0.1000	inverted R-peak	-0.0822

Table 5.4: Estimated gains for focuses F4 and F5.

F4		**F5**	
Max peak	$\hat{G}$	Max peak	$\hat{G}$
0.1485mV	6060.6	0.1393mV	6460.9

The ECG sensor used in our prototypes is based on the AD8232 chipset by Analog Devices [6]. In this chipset the gain is controlled by the ratio between two resistors (Equation 5.3). For both cases, resistance values were then estimated, based on the relation between R_3, R_4, and sensor gain (see Section A.3). For focuses F4 and F5, resistance values could be 100Ω and 500Ω, for R_3 and R_4 respectively. For focuses F1, F2 and F3, resistance values could be 3.2kΩ and 500Ω, for R_3 and R_4 respectively.

$$G = (1 + \frac{R_3}{R_4}) \tag{5.3}$$

For this project, however, such improvements were not implemented due to lack of time. As such, the SmartHeart configuration had an ECG sensor of gain 1100 (see Table 3.1 for BITalino original specifications), and for the R-IoT device, the used ECG sensor had a gain of 5600 (Table 3.1, modified version specifications).

6

Results

6.1 Validation Tests

Initial data acquisition sessions were performed in healthy subjects, in order to test both the setup and the developed prototypes. For this phase of the work, acquisitions were divided into three stages. Firstly, ECG recordings were collected with a medical gold standard, MAC 800 [43]. The following acquisitions were made with only one device at a time, namely the SmarHeart and R-IoT hardware simulators, enabling the data to be sequenced in a short period of time, thus avoiding significant alterations of heart beat waveform between acquisitions. This type of approach prevents any kind of electrical interference between the MAC 800 and the remaining devices. On the other hand, it still allows ECG data collection that is comparable between devices.

In terms of data analysis, the average heartbeat waveform was obtained for each of the twelve leads acquired with the gold standard, and for each of the five auscultations points of both the SmartHeart and R-IoT hardware simulators. The goal was to determine which (if any), and how, leads of the standard ECG have greater morphological resemblance with the data acquired with the non-standard procedures and sensor placements followed in our work.

During these acquisitions, several improvement points were identified. Due to the fragility of the electrodes, it was crucial to make sure their contact with the skin was optimized. Accordingly, when examining male volunteers, androgenic hair made it more difficult to get good electrical contact, which presented differences when female volunteers were auscultated; as mentioned before, physiological factors such as adiposity, body shape, and skin characteristics, may influence the results. Also, as women have breasts, that becomes a situation prone to lower amplitude signals, due to the increased adipose tissue in that area.

Further into the acquisitions, some vulnerabilities were noticed with the R-IoT prototype. Due to the small equipment used, in order to more easily acquire signals on the chest area, contact between the evaluator and metallic parts of the device was practically inevitable. Moreover, even if direct contact was avoided, the small distance from the hand holding the prototype to the ECG sensor interfered with the electrical signal. Distortion was therefore detected when the R-IoT device was held. This was improved by attaching a 10cm PLA rigid 3D printed piece and, as a result, the ECG signal quality was immediately improved. This suggests that the evaluator was acting as a noise source that interacted with, and affected, the quality of the acquired ECG signal. Meticulous isolation of all components of the device is then required in order to obtain an adequate signal.

6.2 SmartHeart Device

After processing all data from the SmartHeart device, values of Euclidean distance, coefficient of determination (R^2) and root mean squared error (RMSE), for each one of the 12 leads, and for each focus, were used to assess the morphological similarity between the heartbeat waveforms. Multiple analysis were performed, in order to better understand the behaviour and correlation between auscultation points and gold standard leads' signals. Throughout this chapter, the underlying processes are further highlighted by plotting the raw data against the filtered ones; as described in Section 5.2.1, R-peaks were detected, and the heartbeat waveforms isolated and analysed, to get a representative description of the morphological pattern in each focus. Figures 6.1, 6.2 & 6.3 illustrate this component.

We also present a plot with both MAC 800 and SmartHeart ECG signals. This was done for each individual lead (I, II, III, aVR, aVL, aVF, V1, V2, V3, V4, V5 & V6) and for each focus (F1, F2, F3, F4 & F5). Mean waves were calculated, as well as the SmartHeart's data standard deviation (depicted as the dotted line in Figure 6.4).

The purpose of evaluating statistical metrics was the identification of the gold standard lead that presents the highest morphological resemblance to each focus signal. In Figure 6.4, for example, it is noticeable the resemblance between leads V1 and V2 (MAC 800), and the SmartHeart signal.

Moreover, numerical analysis was also applied. From the adopted metrics, it is possible to identify a corresponding lead according to the computed values. For

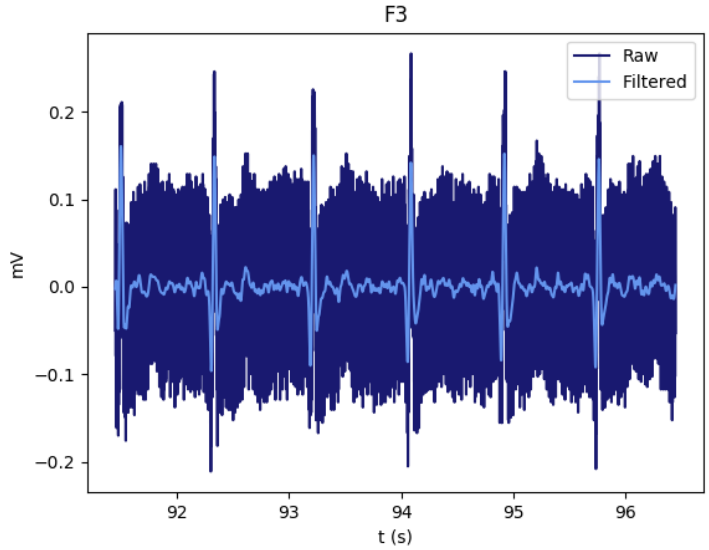

Figure 6.1: Raw *vs.* filtered ECG signal for focus F3 in a case study.

example, for focus F3, in Table B.4, Section B.2, it can be seen that the lowest Euclidean distance and the lowest RMSE points to lead aVL. Furthermore, in Table 6.1, the highest correlation (R^2) is obtained for lead V1.

Considering the setup of the overall data acquisition, the coefficient of determination is the most meaningful value to consider. This is justified by the fact that both the Euclidean distance and RMSE acknowledge distance from point to point, which are generally more sensitive to slight differences in the scaling of the data. As such, we believe to be more adequate to take into consideration R^2 values. Therefore, for this set of results, it can be argued that focus F3 creates a wave similar to lead V1.

To proceed this study, both MAC 800 and SmartHeart heartbeat waveforms were further observed, in search for morphological resemblances. This analysis was crossed with the positioning of electrodes, for each lead and focus. Results can be observed in Table 6.2, where for focuses F1 to F5 one or more lead show similarity, according to the numerical results obtained. With this, the intent was to look for similarities between empirical data and numerical data.

From the numerical results (Table B.4, Section B.4), one could say that F1 resembles more to lead V2, F2 and F3 to lead V1, F4 to lead V4 and F5 to lead I, given the highest R^2 values for each focus.

Often seen throughout the project, focuses F1 to F3 were readily identified with leads V1 or V2. This could be explained by the electrodes' positioning factor involved. The first three focuses are located above the heart, while focuses F4 and F5 are

Table 6.1: SmartHeart device results. R^2 values, for each lead and focus of a case study.

Leads	R^2 **metric values per focus**				
	F1	F2	F3	F4	F5
Lead V5	0.6514	0.7765	0.8408	0.8188	0.6976
Lead V4	0.5945	0.7469	0.8031	**0.8513**	0.7152
Lead V6	0.6996	0.8002	0.8772	0.7561	0.6448
Lead V1	0.8948	**0.8836**	**0.9221**	0.5439	0.4868
Lead II	0.6426	0.7802	0.8459	0.7948	0.6659
Lead V3	0.2070	0.4447	0.4168	0.7916	0.5994
Lead V2	**0.9280**	0.8816	0.8992	0.4469	0.3819
Lead aVL	0.6466	0.5928	0.4726	0.4559	0.4970
Lead aVF	0.6477	0.7929	0.8557	0.7885	0.6524
Lead III	0.6322	0.7875	0.8421	0.8003	0.6533
Lead aVR	0.6401	0.7674	0.8328	0.8004	0.6833
Lead I	0.6044	0.7187	0.7789	0.8306	**0.7325**

Table 6.2: SmartHeart device results. Morphological and positioning analysis for the same case study; ? stands for "can't tell", which happens for bipolar leads; √ stands for similarities found; and "∼" stands for being fairly similar.

	F1	**F2**	**F3**	**F4**	**F5**
Numerical results					
Eucl. distance	aVL	aVL	aVL	aVL	aVL
R^2	V2	V1	V1	V4	I
RMSE	aVL	aVL	aVL	aVL	aVL
Morphological similarities w/ each focus					
aVL	∼	∼	∼	∼	√
V2	√	-	-	-	-
V1	-	∼	√	-	-
V4	-	-	-	X	-
I	-	-	-	-	X
Positioning similarities w/ each focus					
aVL	?	?	?	?	?
V2	√	-	-	-	-
V1	-	√	√	-	-
V4	-	-	-	√	-
I	-	-	-	-	?

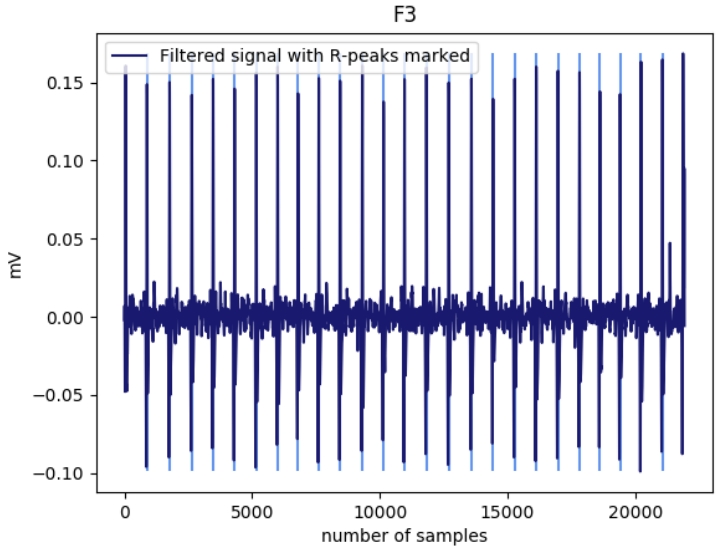

Figure 6.2: R-peaks detection for the same case study, same focus.

below the heart, and more close to it. Similarly, leads V1, V2 and even V3 are acquired at the middle of the chest, also above the heart.

A total of 10 ECG signals were acquired and studied, even though approximately 20 volunteers were considered for this project. This has much to do with setup conditions and specific physiological and anatomical features that prevented some subjects from having a good quality acquisition. Such observations are further explained in Chapter 7.

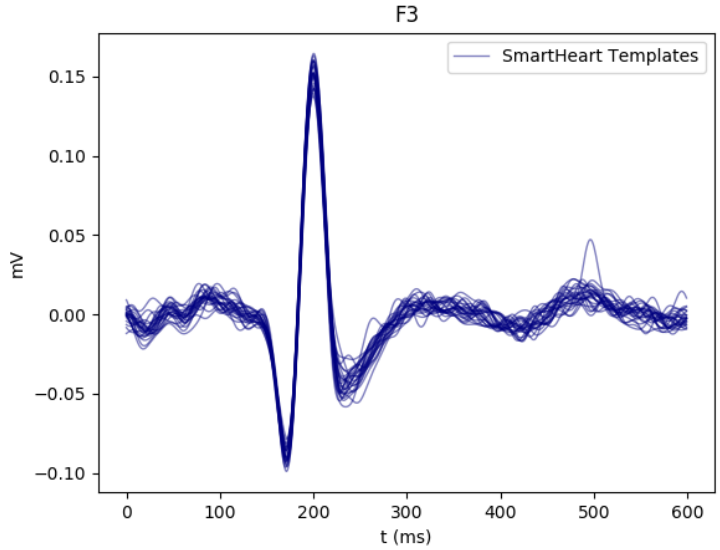

Figure 6.3: Overlapped heartbeat waveforms, for focus F3, same case study as in Figure 6.1 & 6.2.

6.3 R-IoT device

In addition to the SmartHeart prototype, R-IoT data was also processed and analysed. The same set of metrics was adopted: Euclidean distance, R^2 and RMSE, this time for each of the 12 leads, 5 focuses and 4 positions (vertical: 90°; horizontal after 90° rotation clockwise: 0°; vertical after another 90° rotation: -90°; horizontal after a final 90° rotation: -180°). Below are presented the results for another case study, for focus F5. Afterwards, a morphological analysis is also carried, in order to predict which lead resembles more to each position of this focus. This type of reasoning was applied throughout all signals, and all focuses. In the end, this information can be cross linked with SmartHeart results for the same volunteer, in order to verify if the same correlation between focus and lead occurs for both devices.

As before, we also present a plot with both MAC 800 and R-IoT ECG signals. This was achieved for each individual lead (I, II, III, aVR, aVL, aVF, V1, V2, V3, V4, V5 & V6), for each focus (F1, F2, F3, F4 & F5), and each position (90°, 0°, -90° and -180°). Mean waves were calculated, as well as R-IoT's standard deviation (depicted as the dotted line in Figure 6.9).

Taking focus F5 as example, for this case study, numerical results point to leads V1 and V2 as most similar (see R^2 maximum values in Table 6.3, for each different rotation angle). The lowest Euclidean distance values are 84.285, 84.171, 84.428 and

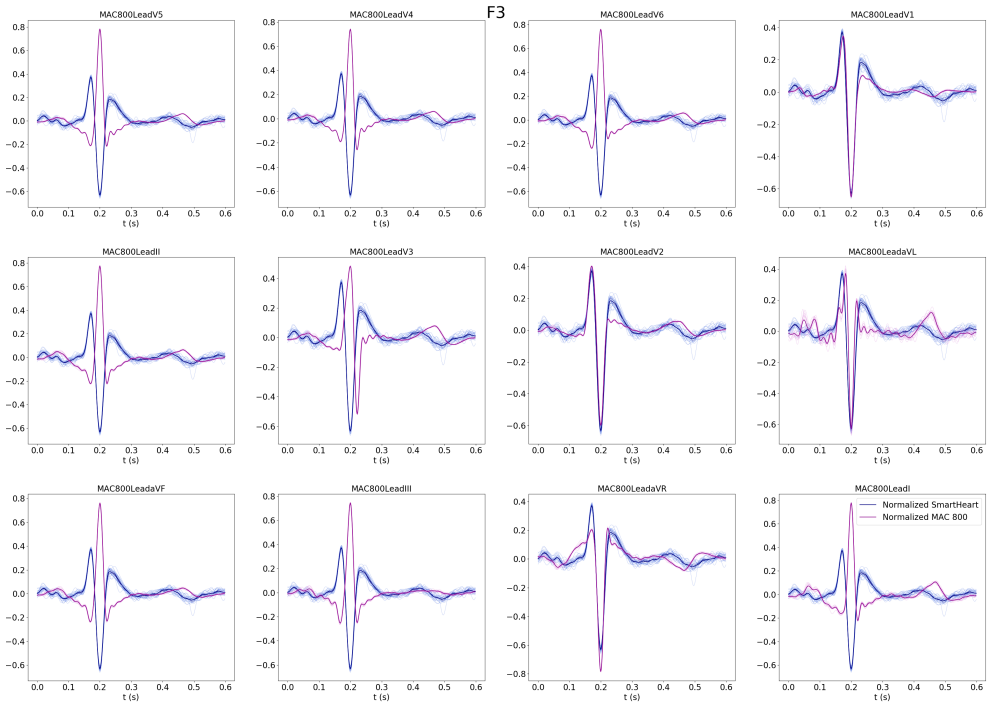

Figure 6.4: Representation of MAC 800 mean waveforms and their templates; SmartHeart heartbeat waveforms and their templates, as well as standard deviation for focus F3.

84.426, for positions 90°, 0°, -90° and -180°, respectively. R^2 maximum values are 0.969, 0.829, 0.933 and 0.967, in the same order; and minimum RMSE values are 7.694, 7.684, 7.707 and 7.707. As mentioned before, R^2 is the most reliable metric for the used setup. Thus, one could come to a conclusion that in focus F5, ECG signals are numerically more similar to lead V1 for a 90°, 0° and -90° position, and lead V2 for a -180° rotation angle, with these leads being the ones which had the higher coefficients of correlation.

Furthermore, when looking to Figure 6.9, one could say that for 90° the most similar waveforms are the ones of leads III and aVF, even though results point to lead V1. Similarly, for 0°, the lead pointed by the numerical analysis does not correspond to the leads morphologically closer to waveforms of the gold standard. This disparity is verified in each rotation angle, from 90° to -180°, due to the coefficient of determination mathematical calculation.

When the R^2 is calculated, it takes into consideration the power of both x and y values, instead of the absolute value. Thus, R^2 values obtained in this context are not invariant to the ECG signal polarity, and, therefore, although several waveforms don't seem morphologically similar to the gold standard leads, the correlation exists

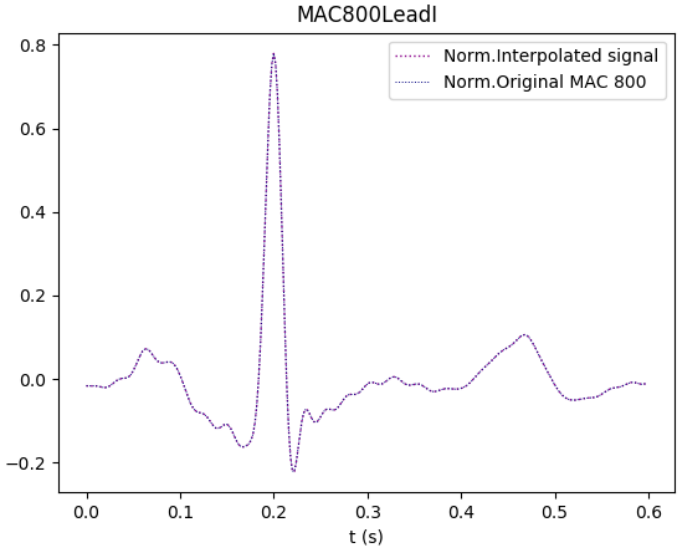

Figure 6.5: Same case study: Example of MAC 800 ECG signal's interpolation for Lead I.

for the symmetric waveform. In sum, the coefficient of correlation and the ECG waveforms presented are, in fact, similar, and lead to the same conclusion regarding what lead better correlates with the gold standard waves.

Another important aspect of this analysis is the influence that rotation angles have in the polarity of the ECG signal. This was the main purpose of using the R-IoT for different angle variations throughout the five medical auscultation points. As expected, inversion of the signal was readily observed when the device changed positions. Given the short time window for this project, further numerical analysis will need to be carried in order to support this evidence in the scope of future work.

For this specific prototype, only few cases were able to be studied. One of the reasons are the many different waveforms to be considered in each acquisition, as it can be perceived by the detailed analysis of the previous R-IoT case study example.

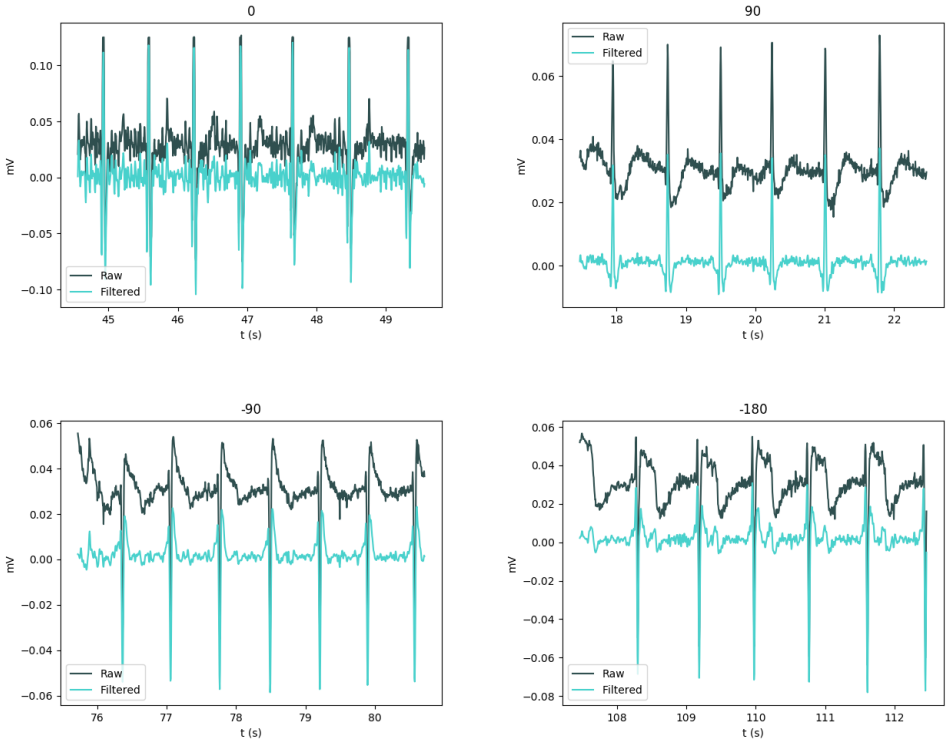

Figure 6.6: Raw *vs.* filtered ECG signal, for focus F5, in a case study.

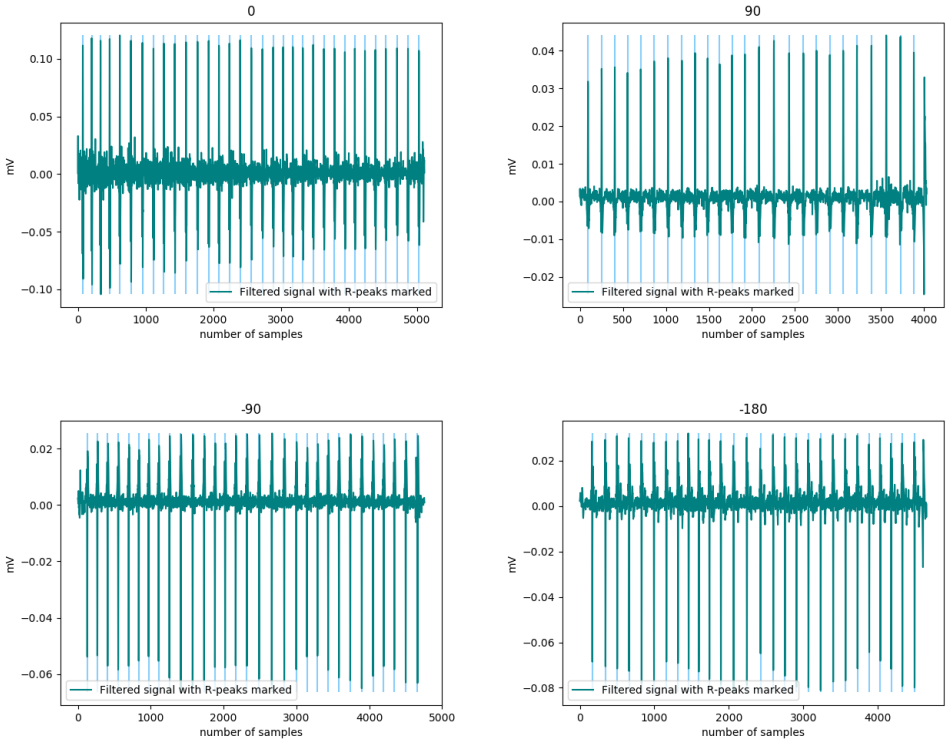

Figure 6.7: R-peaks detection for the same case study, same focus.

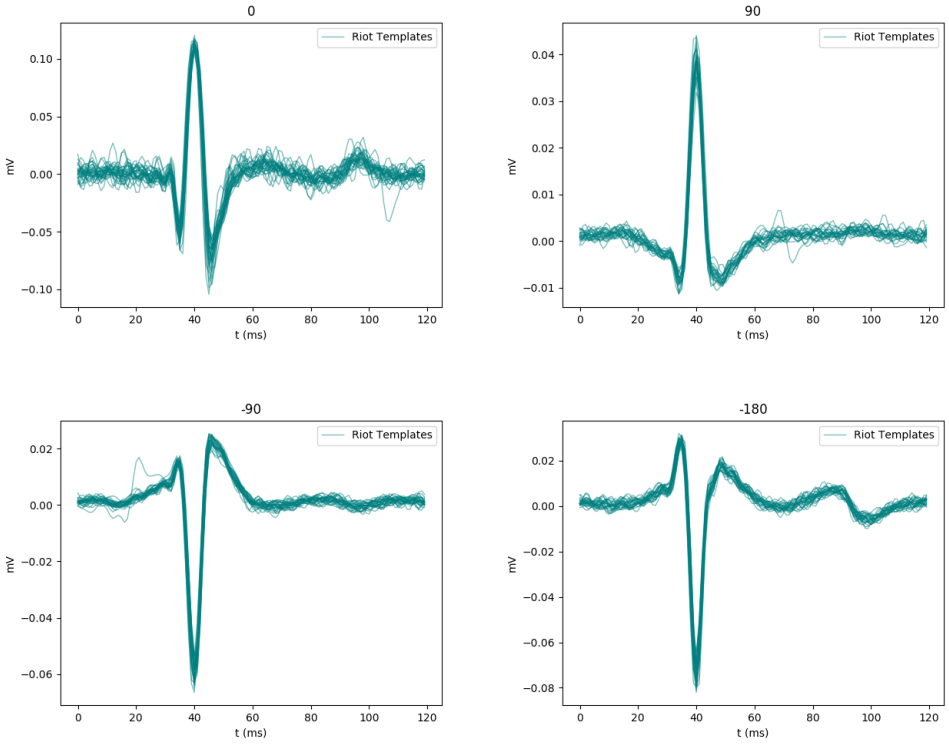

Figure 6.8: Overlapped heartbeat waveforms for focus F5, in the same case study as in Figure 6.6 & 6.7.

Table 6.3: R-IoT device results. Euclidean distance, R^2 and RMSE values for focus F5 and each rotation angle.

Leads	**Focus F5**											
	90°			-90°			-180°			0°		
	Eucl. dist.	R^2	RMSE	Eucl. dist.	R^2	RMSE	Eucl. dist.	R^2	RMSE	Eucl. dist.	R^2	RMSE
Lead V5	392.0817	0.9571	35.7920	392.2716	0.9188	35.8093	392.2890	0.8700	35.8109	391.9289	0.7798	35.7780
Lead V4	268.0300	0.8914	24.4677	268.2137	0.8621	24.4844	268.2264	0.7648	24.4856	267.8849	0.7105	24.4544
Lead V6	376.6808	0.9685	34.3861	376.8717	0.9291	34.4035	376.8901	0.8911	34.4052	376.5258	0.7976	34.3719
Lead V1	382.3215	**0.9695**	34.9010	382.1302	**0.9327**	34.8836	382.1076	0.9497	34.8815	382.4809	**0.8294**	34.9156
Lead II	384.9505	0.9531	35.1410	385.1393	0.9053	35.1582	385.1576	0.8694	35.1599	384.7994	0.7667	35.1272
Lead V3	331.7355	0.8667	30.2832	331.5546	0.8354	30.2667	331.5249	0.9591	30.2639	331.8945	0.7989	30.2977
Lead V2	447.7638	0.9046	40.8751	447.5792	0.8685	40.8582	447.5511	**0.9673**	40.8556	447.9232	0.8116	40.8896
Lead aVL	159.9806	0.8780	14.6042	159.8006	0.8149	14.5877	159.7702	0.9501	14.5850	160.1298	0.7340	14.6178
Lead aVF	362.3731	0.9618	33.0800	362.5625	0.9088	33.0973	362.5835	0.9078	33.0992	362.2209	0.7770	33.0661
Lead III	343.2459	0.9564	31.3339	343.4345	0.8988	31.3511	343.4587	0.9412	31.3533	343.0931	0.7800	31.3200
Lead aVR	219.6753	0.9094	20.0535	219.4904	0.8710	20.0366	219.4771	0.7797	20.0354	219.8219	0.7246	20.0669
Lead I	**84.2850**	0.5337	**7.6941**	**84.4280**	0.5265	**7.7072**	**84.4255**	0.3573	**7.7070**	**84.1712**	0.4343	**7.6837**

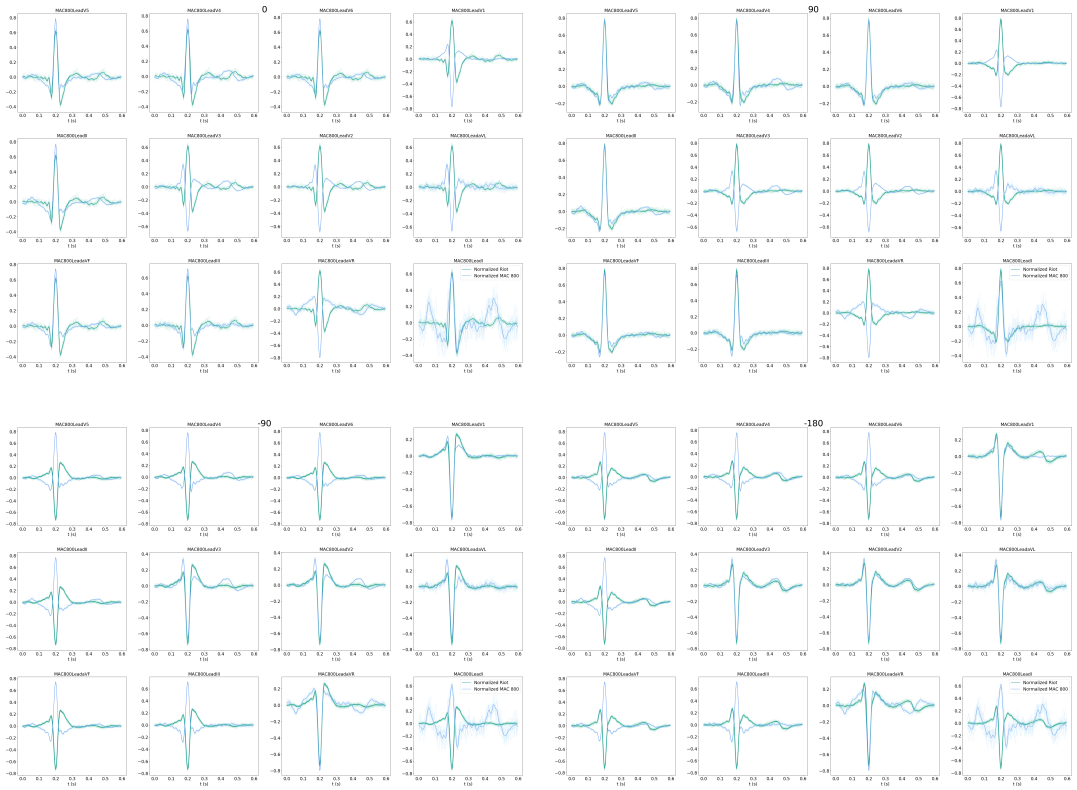

Figure 6.9: Representation of MAC 800 mean waveforms and their templates, for the same case study; R-IoT heartbeat waveforms and their templates, as well as the standard deviation for focus F5. Each quadrant depicts the data for a rotation of the R-IoT.

7

Conclusions

7.1 Summary

In sum, our work has led us to two new prototypes for ECG data acquisition (SmartHeart and R-IoT), to be integrated in a digital stethoscope, which have been validated with a GE MAC 800 gold standard device (see Section 7.2). With this approach, synchronization between ECG and PCG signals, for segmentation and identification of heart sounds, can be achieved, increasing both the accuracy and reliability of the medical diagnosis (see Section 1.2).

Mainly focusing on R^2 values (as explained in Chapter 6), results point to a high correlation between SmartHeart and MAC 800 and, therefore, suggest that ECG signals acquired along the five main auscultation points (focuses F1, F2, F3, F4 & F5) are reliable to support a preliminary diagnosis of heart diseases. From the evaluated population of 10 people throughout this study, there is a pattern found for different groups of focuses (F1, F2 & F3, and F4 & F5). Focuses more distant from the heart, *i.e* F1, F2 & F3, tend to correlate more to leads V1 and V2, which are also the most distant from the heart, considering the 12-Lead ECG. On the other hand, focuses directly around the heart, *i.e* F4 & F5, are usually highly correlated with leads V4, V5 and V6 (also the closest to the heart in a 12-Lead ECG) (see Chapter 6). The waveforms obtained in these focuses are not the same as the ones from a 12-Lead ECG, due to the difference in the electrode placement in each exam, but, according to our results, can be considered similar enough to assist a healthcare professional in assessing irregularities of the heart's electrical activity (see Section 1.1.2).

7.2 Contributions

With this work, several contributions were made, given rise to new devices and a new approach for medical heart examination. Below are the main takeaways.

- SmartHeart device: A small, ergonomic and light weight device, that allows the recording of ECG signals on the chest area, with the electronics incorporated in the footprint of a standard stethoscope; it was developed with the intent of allowing ECG measurements even on auscultation points, having electrophysiological characteristics different than the standard ECG exams.

- R-IoT device: Similarly to SmartHeart, this prototype acts as an ECG recording device, used in auscultation points, differing form the latter in its capacity of angle measurement; with the R-IoT it is possible to study how a simple rotation, while acquiring a signal, can influence its polarity, and the motivation for background of this prototype comes from the fact that more often than not, healthcare professionals freely position the stethoscope on a patient, *i.e*, there's no specific orientation in which the auscultation is carried out, leading to multiple variations in the positioning of the device with respect to the electrical axis of the heart, which introduces variability in the acquired ECG signal waveform.

- ECG validation: This was achieved by comparing a medical gold standard, GE MAC 800, to both the SmartHeart and R-IoT hardware simulators, allowing these prototypes to be recognized as reliable ECG recording devices, and characterizing the waveforms acquired with this unconventional setup.

- Diaphragm materials: As the SmartHeart and R-IoT devices should be able to not only record ECG signals, but also allow auscultation, it was imperative that the material used to integrate the sensors and remaining electronic components, favoured the acoustic conduction; for that, two materials, as well as different diaphragm configurations, were considered and studied, taking into account the constrains of both the PCG and ECG data acquisition.

- Electrode materials: Given the inability to adapt standard Ag/AgCl electrodes on the footprint of a standard stethoscope, alternative materials were researched and used in the developed prototypes, from which a gold alloy was selected.

- Ideation of an accessory for integration of ECG sensing in the 3M Littmann

3200 stethoscope: Collaboration in the work developed by Prof. Ricardo Baptista and Miguel Rocha, from the Polytechnic Institute of Setúbal, in the scope of the BSc final course work of the latter, which resulted in an accessory to integrate the SmartHeart electronics developed in this work on the 3M Littmann 3200 digital stethoscope as a functional and user-friendly form factor (see Figure 7.1).

Figure 7.1: SmartHeart prototype model for ECG integration on a stethoscope.

7.3 Heart Disease Diagnosis

Given the data analysis results, several leads came up as the best representation of each focus or position (here referring to both SmartHeart and R-IoT). Moreover, studying each one of this leads can lead to a preliminary diagnosis, since changes in the obtained waveforms establish some ground principles for heart disease diagnosis. Wave amplitude, wave time, and morphology may vary when certain pathologies manifest in a patient [50].

For example, when there is a left atrial abnormality, which includes atrial dilation, atrial muscular hypertrophy and elevated inter-atrial pressures, changes in the P wave of the ECG for leads II, V1 and V2 can occur. From an extension in time (higher duration than normal), to a shift in its position on the heart axis, or a more prominent notching, the P wave in these leads allows the detection of certain health conditions worth studying more in depth. Likewise, leads aVR, aVL, V1, V2, V5 and V6 would allow the indentification of a right ventricular hypertrophy [51]. More examples are listed in Table 7.1.

Table 7.1: Examples of what pathologies to check for when evaluating each lead.

Heart Diseases	**Leads**
Heart Arrhythmia	II, III, V1, aVF
Right Bundle Branch Block	V1, V2, V3, V6
Left Bundle Branch Block	I, V6

An example of a lead that can be used to control several pathologies is Lead I. It can tell if there is any unconventional behaviour of the waveform, leading to a first suspicion of heart disease. These can be Sinus Tachycardia (sinus rhythm with a rate greater than 120 bpm) and Sinus Bradycardia (sinus rhythm with a rate lower than 60 bpm); Extrasystole (premature contraction of the heart, independent of its normal rhythm); Left Branch Block (delay on the left ventricle activation, causing it to contract later than the right ventricle); Atrioventricular block (total or partial interruption of the electrical impulse from the atria to the ventricles); Tachycardia (heart rate higher than 120 bpm); Escape Rhythms (ventricular rhythm with a rate of 20 to 40 bpm); and pauses (absence of cardiac activity for more than 2 seconds).

In sum, with SmartHeart and R-IoT acquisitions, as one usually extracts information about leads III, I, V1, V2, V5 and V6 (according to Chapter 6), it is possible to identify suspicious behaviours about each wave, potentiating an early initial diagnosis.

7.4 Diaphragms

Regarding the auscultation tests performed, in order to choose the better model to use, in which six different diaphragms were evaluated, results point to the possibility of incorporating the membrane with a solid core (model 191) in this type of devices. As this model presented one of the best evaluations, it shows that it is possible to have adequate performance with a non-standard diaphragm geometry, which also allows for better electronics accommodation inside it. Although the material of all electronic components will certainly influence sound propagation, and therefore the suitability of the model, this leads us to conclude that adequate results will be obtained when all is assembled.

7.5 Future Work

7.5.1 Further Acquisitions

In order to further validate and support the evidence found in this work, more acquisitions should be performed. A wider population should be considered and, as a next stage experiment, both ECG and PCG would be acquired at the same time, with the developed integrated prototype (Figure 7.1). Thus, PCG segmentation, using the corresponding ECG, would be tested and validated.

As future work, it is also proposed that ECG data acquisition with pathological patients are carried out as well. This can lead to a more accurate study of what signals are obtained when the evaluated subject has a heart disease, and also acknowledge if those alterations are significant and suffice for an accurate preliminary diagnosis.

7.5.2 Signal Processing and Analysis

As mentioned in Chapter 6, some of the chosen metrics applied to the acquired signals fell short, regarding the identification of the gold standard lead which most correlated to each focus and angle rotation. As such, for future work it is proposed that additional metrics are studied, namely the cosine distance, in order not to discard the polarity of the ECG waves.

7.5.3 Electrodes

Throughout this project it was seen that skin-electrode contact was not optimal with the developed prototypes (SmartHeart and R-IoT), resulting in noisy signals and increasing the number of case studies in which the ECG could not be used for signal processing. As mentioned in The Handbook of Human Physiological Recording [33], Chapter 4, when electrodes have a small footprint, the electronics must compensate such downfall and amplification should be increased. However, when that happens, noise is also amplified, either from ambient currents in the local environment, or from poor contact.

Therefore, it is suggested that different electrodes are used on these two prototypes. An option would be to use electrodes printed in a desktop 3D printer, and, thus, create a bigger electrode sensing area. These electrodes can have small protrusions,

as depicted in Figure 7.1 (right), to allow overcoming the presence of androgenic hair.

7.5.4 Gain Augmentation Proposal

As shown by the results, when using the SmartHeart simulator around the five auscultation points, the signal acquired was mostly good, showing little to no noise and no saturation whatsoever. However, as previously proposed for R-IoT device, some adjustments to the sensor's gain would be of great use. This would involve increasing the gain for the first three focuses (F1, F2 & F3), with the purpose of having a more user-friendly (and overall data sensitivity) signal amplitude, while maintaining the current gain for focuses F4 & F5. Thus, it is suggested the development of a new version of the SmartHeart ECG sensor; one that enables the dynamic selection of different gains, by means of a digital potentiometer.

Similarly, as signal saturation was detected for both auscultation points F4 and F5, with the R-IoT device (as already discussed in Chapter 6), it is suggested, as proposal for future work, that a digital potentiometer is also used with the R-IoT prototype. Again, this enables the possibility of changing the sensor gain, and better adjust it to different points of examination. Digital potentiometers would communicate with the microcontroler and allow gain change digitally, instead of manually. This way, saturation on F4 & F5 can be avoided and points F1, F2 & F3 can be amplified and better evaluated.

7.5.5 Influence of the Stethoscope Rotation in the ECG Signals

In the scope of this work, only a preliminary study was performed in terms of the influence of the stethoscope rotation. As such, more comprehensive tests should be performed. For example, tests that include a wider range of different rotation angles and a more detailed analysis of their influence on an ECG signal.

Bibliography

[1] A. Castro, P. Gomes, S. S. Mattos, and M. T. Coimbra, "Comparison Between Users of a New Methodology for Heart Sound Auscultation," in *2016 38th Annual International Conference of the IEEE Engineering in Medicine and Biology Society (EMBC)*, pp. 5388–5391, IEEE, aug 2016.

[2] C. OpenStax, *Anatomy and Physiology*. OpenStax, CNX, 2016.

[3] J. Malmivuo and R. Plonsey, *Bioelectromagnetism: Principles and Applications of Bioelectric and Biomagnetic Fields*. New York: Oxford University Press, USA, 1st ed., 1995.

[4] R. E. Klabunde, *Cardiovascular Physiology Concepts*. Lippincott Williams & Wilkins/Wolters Kluwer, 2012.

[5] A. Dupre, S. Vincent, and P. A. Iaizzo, "Basic ECG Theory, Recordings, and Interpretation,"

[6] Devices, Analog, "Datasheet, Single-Lead, Heart Rate Monitor Frontend, AD8232." [Online] `http://www.analog.com/media/en/technical-documentation/data-sheets/AD8232.pdf`, last accessed in 11-06-2018.

[7] WHO, "World Health Organization — Cardiovascular Diseases (CVDs)." [Online] `http://www.who.int/mediacentre/factsheets/fs317/en/`, last accessed in 27-09-2017.

[8] J. Keefer M., "Phonocardiogram Simulator Patent, NASA Technical Reports Server, April 1970." [Online] `https://ntrs.nasa.gov/search.jsp?R=19710015130`, last accessed in 12-06-2017.

[9] A. Moukadem, A. Dieterlen, and C. Brandt, "Phonocardiogram Signal Processing Module for Auto-Diagnosis and Telemedicine Applications," in *eHealth and Remote Monitoring*, InTech, sep 2012.

[10] S. Leng, R. S. Tan, K. T. C. Chai, C. Wang, D. Ghista, and L. Zhong, "The Electronic Stethoscope," *Biomedical Engineering Online*, vol. 14, p. 66, jul 2015.

[11] R. A. O'Rourke, V. Fuster, R. W. Alexander, R. Roberts, S. B. King III, and H. J. Wellens, *O Coração, de HURT'S, Manual de Cardiologia*. Lisboa, Portugal: McGraw-Hill, 10ª ed., 2002.

[12] D. Pereira, A. Castro, P. Gomes, J. Areias, Z. Reis, M. Coimbra, and R. Cruz-Correia, "Encyclopedia of E-Health and Telemedicine - Digital Auscultation: Challenges and Perspectives, Hershey, PA: IGI Global," 2016.

[13] F. Renna, J. Oliveira, and M. T. Coimbra, "A Data-Driven Feature Extraction Method for Enhanced Phonocardiogram Segmentation, CinC, Rennes, France, September 2017," pp. 1–4.

[14] E. K. Chung, *Pocket Guide to ECG Diagnosis*. Oxford: John Wiley and Sons Ltd, 2nd ed., 2001.

[15] S. Meek and F. Morris, "ABC of clinical electrocardiography. Introduction. I-Leads, rate, rhythm, and cardiac axis.," *BMJ (Clinical research ed.)*, vol. 324, pp. 415–8, feb 2002.

[16] Can Ye, B. V. K. V. Kumar, and M. T. Coimbra, "Heartbeat Classification Using Morphological and Dynamic Features of ECG Signals," *IEEE Transactions on Biomedical Engineering*, vol. 59, pp. 2930–2941, oct 2012.

[17] J. Oliveira, C. Oliveira, B. Cardoso, M. S. Sultan, and M. Tavares Coimbra, "A multi-spot exploration of the topological structures of the reconstructed phase-space for the detection of cardiac murmurs," in *2015 37th Annual International Conference of the IEEE Engineering in Medicine and Biology Society (EMBC)*, pp. 4194–4197, IEEE, aug 2015.

[18] C. Ye, B. K. V. Kumar, and M. T. Coimbra, "An Automatic Subject-Adaptable Heartbeat Classifier Based on Multiview Learning," *IEEE Journal of Biomedical and Health Informatics*, vol. 20, pp. 1485–1492, nov 2016.

[19] W. Phanphaisarn, A. Roeksabutr, P. Wardkein, J. Koseeyaporn, and P. Yupapin, "Heart detection and diagnosis based on ECG and EPCG relationships.," *Medical devices (Auckland, N.Z.)*, vol. 4, pp. 133–44, 2011.

[20] Littmann, Brand 3M, "3M Littmann Manual: Electronic Stethoscope Model 3200." [Online] `https://multimedia.3m.com/mws/media/594115O/`

3m-littmann-electronic-stethoscope-model-3200-user-manual.pdf, last accessed in 08-06-2018.

[21] C. S. A. Pinto, "A Comparative Study of Electronic Stethoscopes, FMUP Dissertation," December 2015.

[22] C. Dan, W. He, J. Zhou, and X. Li, "Playing and acquiring heart sounds and electrocardiogram simultaneously based on LabVIEW," *Automation Congress, 2008. WAC 2008. World*, pp. 1–4, 2008.

[23] M. E. Bravo-Zanoguera, Z. Y. Medrano, M. A. Reyna-Carranza, R. Lopez-Avitia, and H. Arriola, "Simultaneous capture and display of electrocardiogram and multi-site phonocardiogram," *2009 Pan American Health Care Exchanges - PAHCE 2009*, pp. 26–28, 2009.

[24] J. C. G. Alvarez, "ECG-PCG Simultáneo (SCG): Un viejo-nuevo método para diagnóstico del corazón," August 2000.

[25] N. K. Al-qazzaz, I. F. Abdulazez, and S. A. Ridha, "Simulation Recording of an ECG, PCG, and PPG for Feature Extractions," vol. 10, no. 4, pp. 81–91, 2014.

[26] DUO, "Eko DUO Stethoscope + EKG." [Online] https://ekodevices.com/duo/, last accessed in 03-10-2017.

[27] Rijuven, "CardioSleeve." [Online] https://rijuven.com/medicaldevices/cardiosleeve, last accessed in 03-10-2017.

[28] C. Landgraf, E. Gershtein, and T. Crouch, "Enhanced wireless communication for medical devices - Eko DUO Patent, 2017." [Online] https://www.google.com/patents/US9736625, last accessed in 11-10-2017.

[29] R. Kapoor, "Mobile front-end system for comprehensive cardiac diagnosis - CardioSleeve Patent, 2015." [Online] https://www.google.com/patents/US20150065814, last accessed in 11-10-2017.

[30] S. K. Nayak, D. Biswal, B. Champaty, K. Pal, A. Anis, B. Mohapatra, and D. N. Tibarewala, "Development of a simultaneous acquisition system for ECG, PCG and body temperature signals," in *2015 Annual IEEE India Conference (INDICON)*, pp. 1–6, IEEE, dec 2015.

[31] S. Ummadisetty, B. K. Biswal, and S. S. Ray, "A portable system for simultaneous acquisition of ECG and PCG in real time," in *2014 International Con-*

ference on Power, Control and Embedded Systems (ICPCES), pp. 1–4, IEEE, dec 2014.

[32] M. Jimeno, Y. de la Hoz, and J. Wilches, "Wireless ECG and PCG Portable Telemedicine Kit for Rural Areas of Colombia," *Investigacion e Innovación en Ingenierias*, vol. 2, no. 2, pp. 1–9, 2014.

[33] Macy, A., "The Handbook of Human Physiological Recording, 4: Electrodes." [Online] `http://alanmacy.com/chapter/chapter-4-electrodes/`, last accessed in 09-03-2018.

[34] C. J. De Luca, *Muscles Alive: Their Functions Revealed by Electromyography, Chapter Apparatus, Detection, and Recording Techniques.* Williams & Wilkins, 1985.

[35] M. Puurtinen, J. Viik, and J. Hyttinen, "Best electrode locations for a small bipolar ECG device: Signal strength analysis of clinical data," *Annals of Biomedical Engineering*, vol. 37, no. 2, pp. 331–336, 2009.

[36] M. Puurtinen, J. Hyttinen, and J. Malmivuo, "Optimizing bipolar electrode location for wireless ECG measurement-analysis of ECG signal strength and deviation between individuals," *International Journal of Bioelectromagnetism*, vol. 1, no. 1, pp. 236–239, 2005.

[37] Smith, S. W., "The Scientist and Engineer's Guide to Digital Signal Processing, Chapter 3 - ADC and DAC." [Online] `https://www.dspguide.com/ch3/1.htm`, last accessed in 26-02-2018.

[38] S. Carrara and K. Iniewski, *Handbook of Bioelectronics, Directly Interfacing Electronics and Biological Systems.* Cambridge University Press, 2015.

[39] Lee, S. and Kruse, J., "Biopotential Electrode Sensors in ECG/EEG/EMG Systems." [Online] `https://www.analog.com/MedicalICs`, last accessed in 08-03-2018.

[40] H. P. da Silva, C. Carreiras, A. Lourenço, A. Fred, R. C. das Neves, and R. Ferreira, "Off-the-person electrocardiography: performance assessment and clinical correlation," *Health and Technology*, vol. 4, pp. 309–318, apr 2015.

[41] H. P. Silva, "BITalino: A Novel Hardware Framework for Physiological Computing," *Proceedings of the International Conference on Physiological Computing Systems*, pp. 246–253, 2014.

[42] H. P. da Silva and A. Fred, "Biosignals for Everyone," pp. 64–71, 2014.

[43] "GE Healtcare, MAC 800 resting ECG - Technical Specifications," 2012.

[44] Stethoscope, Littmann, "3M^{TM} Littmann® Electronic Stethoscope Model 3200." [Online] `https://www.littmann.com/3M/en_US/littmann-stethoscopes/products/`, last accessed in 17-10-2017.

[45] M. R. Neuman, *The Biomedical Engineering Handbook: Second Edition, Chapter: Biopotential Electrodes*. Boca Raton: CRC Press LLC, 2000.

[46] E. J. D. Bronzino, "Neuman, M. R. "Biopotential Electrodes."," *Medical Instrumentation: Application and Design*, p. 713, 2010.

[47] A. Koklu, A. C. Sabuncu, and A. Beskok, "Rough Gold Electrodes for Decreasing Impedance at the Electrolyte/Electrode Interface," vol. 21, no. 2, pp. 129–139, 2017.

[48] H. P. da Silva, A. Lourenço, A. Fred, and R. Martins, "BIT: Biosignal Igniter Toolkit," *Computer Methods and Programs in Biomedicine*, vol. 115, no. 1, pp. 20–32, 2014.

[49] P. Hamilton and E. P. Limited, "Open Source ECG Analysis," pp. 101–104, 2002.

[50] J. C. M. Rodrigues, *Electrocardiografia Clínica - Princípios Fundamentais*. Lisboa, Portugal: Lidel - EdiçõesTécnicas, Lda., 2ª ed., 2010.

[51] D. P. Zipes, R. O. Bonow, D. L. Mann, and G. F. Tomaselli, *Braunwald's Heart Disease E-Book: A Textbook of Cardiovascular Medicine*. 11th ed., 2018.

Appendices

A

Experimental Setup and Data Acquisition

A.1 Experimental Protocol

Protocol proposal for physiological data collection - SmartHeart Project

Mónica Martins, Hugo Silva and Ana Fred

In order to evaluate the performance of SmartHeart Project's device, we aim to acquire Electrocardiography (ECG) signals, in healthy subjects, through an auscultation-like technique. In this document it is described each biosensor's position, acquisition times and all features involved. The combination of both Phonocardiogram (PCG) and ECG exams has multiple advantages. More specifically, this work focuses on mapping PCG signals' segments, as well as in eliminating possible outliers, due to the facility of R peaks detection. This way, it becomes possible to evaluate the cardiac dynamics during a standard auscultation (PCG) exam, bringing a novel approach to a general practitioner doctor's appointment, and assisting in the complementary exam prescription process. The importance of such practice relies on the fact that an electrocardiogram is only taken under medical prescription and that PCG is a standard medical exam in general medicine.

Acquisition device - BITalino and MAC 800: Our experimental device is based on the BITalino platform, which allows the measurement of one lead ECG data by means of a local differential bipolar approach. Specifications of the ECG sensor are presented in Table 1.

Table 1: Specifications of the ECG sensor.

Specification	Values
Measurement Range	0.33mV
Bandpass Filtering	1-30Hz
Input Impedance	>1MOhm
CMRR	110dB
Gain	5600

The transfer function of the ECG sensor is given by Equation (1). The ADC value is the value sampled from the channel; 2^n is 1024 for the BITalino channels (given the 10-bit resolution); VCC (the operating voltage) is 3.3V and the denominator is the ECG gain, 5000. The ECG value is in the range $[-0.33mV, 0.33mV]$.

$$V_{ECG} = \frac{(\frac{ADC}{2^n} - \frac{1}{2}) \times VCC}{5000} \quad (1)$$

As mentioned, raw ECG signals will be acquired with a customized version of BITalino, used in a 10 bit resolution and $1KHz$ sampling frequency configuration. Table 2 describes the main specifications of the biosignal acquisition unit.

Table 2: Specifications of the BITalino device.

Specification	Value
Wireless Range	up to 10 m
Resolution	up to 10-bit
Sampling Rate	up to 1000Hz
Weight	74g
Size	84×53×18 mm
Battery	Li-On; 7.4V; 500mAh

This new personalized BITalino was created taking into account the auscultation process, hence the round and stethoscope-like shape, as seen in Figure 1. Around the plastic cap, an Au-Ag alloy functions as the electrode, and a knob was also added, in order to facilitate the handling. Inside this structure is where the sensor itself is placed.

The goal of our study is to perform sequential data acquisition with GE Healthcare MAC 800 Resting ECG (Figure 2) in a 12-lead (or more) ECG configuration exam, so that this information can be used as a gold standard ECG to benchmark our sensor set-up against.

Physiological signals:

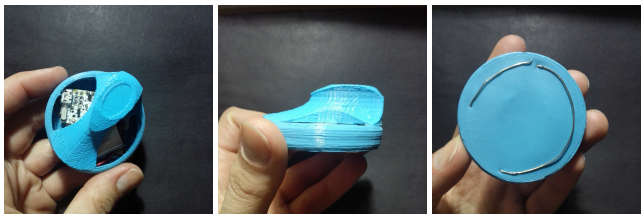

(a) (b) (c)

Fig. 1. SmartHeart prototype device.

Fig. 2. Gold Standard - GE Healthcare MAC 800 Resting ECG

12-lead Electrocardiogram (ECG)

With this experiment we intend to measure a 12-lead ECG in healthy controls, making acquisitions of all six precordial leads (depicted in Figure 3 by points V1 to V6), and the remaining 6 leads: aVR, aVL, aVF (augmented unipolar leads), DI, DII and DIII (bipolar leads).

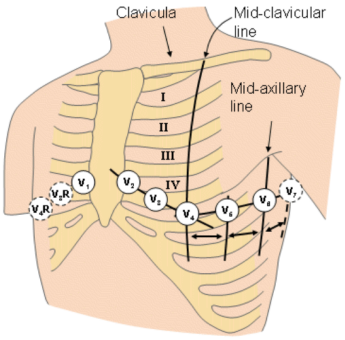

Fig. 3. 12 leads ECG positions [1]

Digital record of the Electrocardiogram (ECG)

Although the measurement itself already gives important information, it is also necessary to perform some data analysis over the acquired signals. For this reason we will need the digital version of the recordings. This allows us to use computation processes like filtering, correlation and error calculus, among others, giving space for statistical studies and, most importantly, to evaluate the performance of this new device.

Phonocardiogram auscultation points

Phonocardiogram (PCG) is used as a complementary exam of auscultation, given that the latter relies on the human ear, which may not be sufficient for an accurate evaluation of the patient. The main problem with this technique is that it's difficult to master, hence the importance of using digital stethoscopes (auscultation and phonocardiography).

The PCG exam provides information about the heart activity, through its sounds, which are in the range of 10 to 750 Hz, and therefore being low frequency. With PCG it is possible to know the temporal localization of the heart sounds, the number of their internal components, their frequency content and the significance of diastolic and systolic murmurs, with these

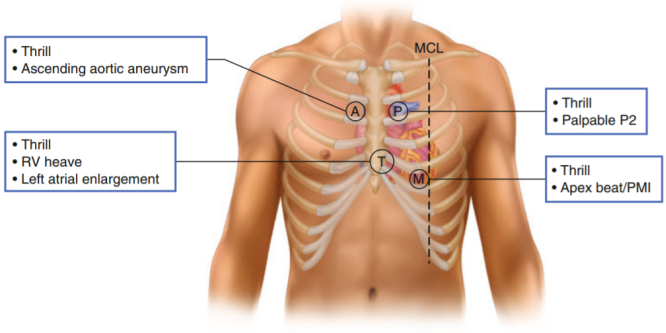

Fig. 4. PCG acquisition points [2]

being an extra or unusual sound heard during a heartbeat and broadly classified as systolic, diastolic and continuous.

The points where the auscultation should be carried are marked in Figure 4 and each point should take about one minute to be properly analysed.

Conclusion: In conclusion, this protocol aims to present an overview of the data acquisition protocol to be carried, in order to collect data to benchmark an experimental device being developed in the scope of the SmartHeart Project. The work attempts to develop a new biomedical data acquisition device configuration that can evaluate a patient's heart condition both through ECG and PCG at the same time.

Acknowledgment: This work was partially supported by the IT - Instituto de Telecomunicações under the grant UID/EEA/50008/2013 "SmartHeart".

References

1 Malmivuo, Jaako and Plonsey, Robert: 'Bioelectromagnetism: Principles and Applications of Bioelectric and Biomagnetic Fields', *Oxford University Press, USA*, 1995, chapter 15
2 Kusko M.C., Maselli K. (2015) Introduction to Cardiac Auscultation. In: Taylor A. (eds) Learning Cardiac Auscultation. Springer, London

A.2 Informed Consent

Consentimento informado

Autor: Mónica Martins, aluna no Mestrado Integrado em Engenharia Biomédica da Faculdade de Ciências e Tecnologias, da Universidade de Coimbra

O projeto de mestrado "Towards an Integrated Electrocardiography System for digital Stethoscopes", insere-se num estudo que decorre no âmbito do Mestrado Integrado em Engenharia Biomédica, em articulação com o Instituto de Telecomunicações do Instituto Superior Técnico, e tem como principal objetivo desenvolver um dispositivo que permita a aquisição de sinais de eletrocardiograma (ECG) nos cinco focos principais de auscultação médica.

Dado o conceito inovador de associação de ECG com auscultação, este projeto exige um processo inicial de validação do sinal, sendo, para isso, necessária a colaboração de voluntários saudáveis. É de salientar que com a sua colaboração estará, não só a contribuir para a realização deste projeto de investigação, mas também para um maior conhecimento na área científica, promovendo a elaboração e implementação de sistemas de comunicação alternativa e aumentativa na área da saúde, que poderão beneficiar pacientes no futuro.

Este estudo encontra-se, por sua vez, integrado num trabalho de maior dimensão, envolvendo outros grupos de investigação, que pretende que este dispositivo venha a ser integrado num estetoscópio digital. Com isto, temos então um único aparelho médico que permite obter sinais de fonocardiograma (sons cardíacos) e de eletrocardiograma (sinal elétrico do coração) numa mesma aquisição, aumentando, assim, a qualidade do diagnóstico médico.

Informa-se que a recolha de dados será feita no Instituto de Telecomunicações, recorrendo aos equipamentos: Eletrocardiógrafo MAC 800, BITalino e R-IoT. Todos os dados recolhidos serão anonimizados, e não serão publicadas quaisquer imagens adquiridas. No entanto, os registos poderão vir a ser partilhados com outros profissionais para efeitos de investigação.

Em qualquer momento do estudo é livre de desistir, se assim o pretender. A sua participação é voluntária, sem qualquer contrapartida ou risco.

Se existirem dúvidas, por favor contacte a investigadora Mónica Martins, através do *e-mail*: monica.cm-martins@gmail.com ou telemóvel: +351 919 610 960.

"Declaro ter compreendido os objetivos que me foram propostos e explicados. Foi-me concedida a oportunidade de esclarecer as dúvidas sobre o assunto e garantido que não haverá prejuízo para os meus direitos assistenciais se eu recusar esta solicitação.

Autorizo o ato indicado neste documento.”

Data: ___/ ___ / _____

(Utente/ Responsável)	(Aluno)

A.3 ECG Sensor Chipset

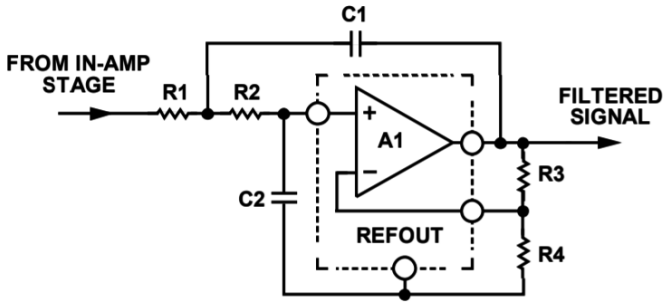

Figure A.1: Electronic circuit diagram for the ECG sensor used in the SmartHeart and R-IoT prototypes: R_3 and R_4 relation to sensor gain. Image from [6].

B

Comprehensive Results Listing

B.1 Further Segmentation for Signal Amplitude Characterization

Table B.1: Segmentation of all four different diaphragm positions, for both focus F4 and F5.

Segmentation indexes																
F4								**F5**								
90º		**0º**		**-90º**		**-180º**		**90º**		**0º**		**-90º**		**-180º**		
x_s	1610.83	x_s	6927.57	x_s	12704.70	x_s	17501.10	x_s	836.14	x_s	7625.72	x_s	14615.30	x_s	19708.60	
x_e	6165.70	x_e	10976.60	x_e	16655.70	x_e	22332.00	x_e	5967.80	x_e	12974.50	x_e	18520.60	x_e	25231.30	

B.2 Metrics Results for Each Focus

Below is depicted further information regarding the SmartHeart device metrics' results.

Focus F1: The lowest value of Euclidean distance corresponds to lead aVL; the maximum value for R^2 corresponds to lead V2; and the lowest RMSE is the one of lead aVL (Table B.2).

Focus F2: The lowest value of Euclidean distance corresponds to lead aVL; the maximum value for R^2 corresponds to lead V1; and the lowest RMSE is the one of lead aVL (Table B.3).

Focus F3: The lowest value of Euclidean distance corresponds to lead aVL; the maximum value for R^2 corresponds to lead V1; and the lowest RMSE is the one of lead aVL (Table B.4).

Focus F4: The lowest value of Euclidean distance corresponds to lead aVL; the maximum value for R^2 corresponds to lead V4; and the lowest RMSE is the one of lead aVL (Table B.5).

Focus F5: The lowest value of Euclidean distance corresponds to lead aVL; the maximum value for R^2 corresponds to lead I; and the lowest RMSE is the one of lead aVL (Table B.6).

Table B.2: Euclidean distance, coefficient of correlation and RMSE metric values for Focus F1.

Leads	**Focus F1**		
	Eucl. Distance	R^2	RMSE
Lead V5	939.292	0.651	38.378
Lead V4	807.542	0.594	32.995
Lead V6	769.901	0.699	31.457
Lead V1	692.689	0.894	28.302
Lead II	922.298	0.642	37.684
Lead V3	587.403	0.207	24.000
Lead V2	658.761	**0.928**	26.916
Lead aVL	**141.872**	0.646	**5.796**
Lead aVF	699.848	0.647	28.595
Lead III	490.636	0.632	20.046
Lead aVR	690.308	0.640	28.205
Lead I	474.385	0.604	19.382

Table B.3: Euclidean distance, coefficient of correlation and RMSE metric values for Focus F2.

Leads	**Focus F2**		
	Eucl. Distance	R^2	RMSE
Lead V5	939.427	0.776	38.384
Lead V4	807.681	0.747	33.001
Lead V6	770.032	0.800	31.463
Lead V1	692.577	**0.884**	28.298
Lead II	922.435	0.780	37.690
Lead V3	587.561	0.445	24.007
Lead V2	658.655	0.882	26.912
Lead aVL	**141.791**	0.593	**5.793**
Lead aVF	699.988	0.793	28.601
Lead III	490.778	0.787	20.053
Lead aVR	690.174	0.767	28.200
Lead I	474.514	0.719	19.388

Table B.4: Euclidean distance, coefficient of correlation and RMSE metric values for Focus F3.

Leads	**Focus F3**		
	Eucl. Distance	R^2	RMSE
Lead V5	939.697	0.841	38.395
Lead V4	807.944	0.803	33.012
Lead V6	770.310	0.877	31.474
Lead V1	692.303	**0.922**	28.287
Lead II	922.706	0.846	37.701
Lead V3	587.729	0.417	24.014
Lead V2	658.390	0.899	26.901
Lead aVL	**141.642**	0.473	**5.787**
Lead aVF	700.259	0.856	28.612
Lead III	491.045	0.842	20.064
Lead aVR	689.905	0.833	28.189
Lead I	474.774	0.779	19.399

Table B.5: Euclidean distance, coefficient of correlation and RMSE metric values for Focus F4.

Leads	**Focus F4**		
	Eucl. Distance	R^2	RMSE
Lead V5	939.684	0.819	38.394
Lead V4	807.960	**0.851**	33.012
Lead V6	770.255	0.756	31.472
Lead V1	692.475	0.544	28.294
Lead II	922.681	0.795	37.700
Lead V3	587.910	0.792	24.021
Lead V2	658.605	0.447	26.910
Lead aVL	**141.655**	0.456	**5.788**
Lead aVF	700.227	0.789	28.611
Lead III	491.024	0.800	20.063
Lead aVR	689.923	0.800	28.189
Lead I	474.792	0.831	19.399

Table B.6: Euclidean distance, coefficient of correlation and RMSE metric values for Focus F5.

Leads	**Focus F5**		
	Eucl. Distance	R^2	RMSE
Lead V5	939.144	0.698	38.372
Lead V4	807.409	0.715	32.990
Lead V6	769.737	0.645	31.451
Lead V1	692.912	0.487	28.312
Lead II	922.148	0.666	37.678
Lead V3	587.371	0.599	23.999
Lead V2	659.003	0.382	26.926
Lead aVL	**142.042**	0.497	**5.804**
Lead aVF	699.696	0.652	28.589
Lead III	490.488	0.653	20.041
Lead aVR	690.456	0.683	28.211
Lead I	474.251	**0.732**	19.377

Table B.7: Average metrics values per lead.

Leads	**Average per lead**					
	Eucl. Distance	Std	R^2	Std	RMSE	Std
Lead V5	939.4489	0.2164	0.7570	0.0720	38.3848	0.0088
Lead V4	807.7072	0.2175	0.7422	0.0874	33.0020	0.0089
Lead V6	770.0473	0.2145	0.7556	0.0802	31.4633	0.0088
Lead V1	692.5913	0.2046	0.7462	0.1898	28.2985	0.0084
Lead II	922.4537	0.2160	0.7459	0.0783	37.6904	0.0088
Lead V3	587.5949	0.2024	0.4919	0.1952	24.0085	0.0083
Lead V2	658.6828	0.2007	0.7075	0.2407	26.9131	0.0082
Lead aVL	141.8006	0.1483	0.5330	0.0740	5.7938	0.0061
Lead aVF	700.0037	0.2165	0.7474	0.0830	28.6014	0.0088
Lead III	490.7942	0.2168	0.7431	0.0842	20.0533	0.0089
Lead aVR	690.1531	0.2148	0.7448	0.0722	28.1989	0.0088
Lead I	474.5436	0.2127	0.7330	0.0753	19.3893	0.0087